

Facies Analysis, Sequence Stratigraphy and Diagenetic Studies of the Jurassic Carbonates of the Kohat Basin, Northwest Pakistan: Reservoir Implications



1922—2022

Emadullah KHAN^{1, 2}, Abbas Ali NASEEM^{1, *}, Suleman KHAN³, Bilal WADOOD^{4, 5}, Faisal REHMAN¹, Maryam SALEEM⁶, Mubashir MEHMOOD², Waqar AHMAD⁷, Zubair AHMED² and Tahir AZEEM¹

¹ Department of Earth Sciences, Quaid-e-Azam University, Islamabad 45320, Pakistan

² Department of Geology, Abdul Wali Khan University, Mardan 23200, Pakistan

³ Department of Geology, University of Peshawar, Peshawar 24420, Pakistan

⁴ State Key Laboratory of Continental Dynamics, Department of Geology, Northwest University, Xi'an 71006, China

⁵ Department of Geology, University of Swabi, Swabi 23561, Pakistan

⁶ Department of Earth & Environmental Sciences, Bahria University, Islamabad 44000, Pakistan

⁷ Department of Earth & Atmospheric Sciences, University of Alberta, Edmonton T6G 2R3, Canada

Abstract: The present study deals with the depositional facies, diagenetic processes and sequence stratigraphy of the shallow marine carbonates of the Samana Suk Formation, Kohat Basin, in order to elucidate its reservoir quality. The Samana Suk Formation consists of thin to thick-bedded, oolitic, bioclastic, dolomitic and fractured limestone. Based on the integration of outcrop, petrographic and biofacies analyses, the unit is thought to have been deposited on a gentle homoclinal ramp in peritidal, lagoonal and carbonate shoal settings. Frequent variations in microfacies based sea-level curve have revealed seven Transgressive Systems Tracts (TSTs) and six Regressive Systems Tracts (RSTs). The unit has undergone various stages of diagenetic processes, including mechanical and chemical compaction, cementation, micritization, dissolution and dolomitization. The petrographic analyses show the evolution of porosity in various depositional and diagenetic phases. The fenestral porosity was mainly developed in peritidal carbonates during deposition, while the burial dissolution and diagenetic dolomitization have greatly enhanced the reservoir potential of the rock unit, as is further confirmed by the plug porosity and permeability analyses. The porosities and permeabilities were higher in shoal facies deposited in TSTs, as compared to lagoonal and peritidal facies, except for the dolomite in mudstone, deposited during RSTs. Hence good, moderate and poor reservoir potential is suggested for shoal, lagoonal and peritidal facies, respectively.

Key words: porosity, diagenesis, reservoir, Samana Suk Formation, Kohat Basin

Citation: Khan et al., 2022. Facies Analysis, Sequence Stratigraphy and Diagenetic Studies of the Jurassic Carbonates of the Kohat Basin, Northwest Pakistan: Reservoir Implications. *Acta Geologica Sinica (English Edition)*, 96(5): 1673–1692. DOI: 10.1111/1755-6724.14938

1 Introduction

Carbonate reservoirs host 60% of global oil and 40% of the planet's gas reserves, including the world's largest oil field of Ghawar, Saudi Arabia (Scoffin, 1987; Montaron, 2008; Kakemem et al., 2021). Nevertheless, predicting the reservoir potential of these rocks is quite challenging, due to their complexity and heterogeneity when compared with clastic strata (Nazari et al., 2019). The causes of the spatial and temporal variability in the petrophysical properties (porosity and permeability) of the carbonates are due to changes in depositional and diagenetic environments, as well as their subsequent modification by tectonic activity. The primary porosities within carbonates are controlled by packing, sorting and grain-size, which varies according to the depositional environment of the rocks (Ali et al., 2018). The depositional environment also

controls the primary mineralogy of the carbonate rocks, which subsequently controls the diagenetic modifications and hence the secondary porosity of the rocks (Worden et al., 2018). Likewise, diagenesis controls the evolution of secondary porosity within carbonate rocks at various stages i.e. eogenetic (beginning on the sea-floor), mesogenetic (burial) and telogenetic (uplift period; Choquette and Pray, 1970). The compaction, microbial micritization, neomorphism, dissolution/precipitation, replacement and dolomitization in these stages cause changes to the primary fabric, composition, rigidity as well as the porosity (Flügel, 2004). The marked changes in the pore size and shape during diagenesis either enhances or obliterates the reservoir quality (Watney et al., 1998; Taylor et al., 2010; Amel et al., 2015; Afife et al., 2017). Porosity evolution in carbonate rocks correlates with sea-level fluctuations (Morad et al., 2000; Flügel, 2004), e.g. porosity occludes as a result of heavy cementation during regression in large-size pore systems while deposition of

* Corresponding author. E-mail: abbasaliqau@gmail.com

matrix-supported lithologies preserves higher primary porosities during transgression (Read and Horbury, 1993; Tucker, 1993; Flügel, 2004). The transgressive/regressive cycles control the size and proportions of carbonate grains, the chemistry of the pore water as well as the residence time of a particular diagenetic process, which consequently controls the pore system (Morad, 1998; Morad et al., 2012). The shallow to marginal marine conditions are marked by frequent changes in accommodation space, as a result of transgressive and regressive cycles and hence it causes the deposition of shallow to marine facies, with pronounced spatial and temporal heterogeneity in the pore system (Emery and Myers, 1996; Hillgärtner and Strasser, 2003).

The Middle Jurassic carbonates are the best analog of such shallow to marine carbonates. Such carbonates are widely distributed in the adjacent continents e.g. oolitic peritidal carbonates are reported from the Arab Formation, southern UAE (Hollis et al., 2017). Similarly, the Middle Jurassic portion of the Sahtan Group is also comprised of oolitic shoals to lagoonal carbonates in central Oman (Rousseau et al., 2005). Likewise, synchronous deposition of marginal to shallow marine carbonates is reported from the Dhurma Formation of central Saudi Arabia and the Central High Atlas of Morocco (Purser and Evans, 1973; Addi and Chafiki, 2013; Yousif et al., 2018). Such Middle Jurassic carbonates are not restricted to the region but show a global distribution e.g. Middle Jurassic carbonates are deposited in the Lusitanian Basin, Portugal (Azerêdo et al., 2020), oolitic shoal facies within the Great Oolite Group of England (Sellwood et al., 1985), oolitic shoal facies of the Jaisalmir Formation, India, Switzerland and Antalya, Turkey (Ayyıldız et al., 2001; Wetzel et al., 2013; Ahmad et al., 2020). Likewise, synchronous shallow marine oolitic shoals to lagoonal carbonates are also reported from the Paris Basin, France, as well as the Bucegi Mountains, Southern Carpathians, Romania (Brigaud et al., 2009; Lazăr et al., 2013). Such shallow to marine carbonates carry great hydrocarbon potential, e.g. the carbonate shoals constitute very good reservoirs (Ding et al., 2019), the reservoir quality decreasing landward in the lagoon and peritidal settings as well as in deeper conditions below the wave base (Flügel, 2004; Kakemem et al., 2021). However, the diagenetic modification of such units can be very productive (Wadood et al., 2021a). The shallow to marginal marine carbonates of the Middle Jurassic are widely deposited in the Indus Basin of Pakistan. Amongst these, the Samana Suk Formation is best exposed in the Upper Indus Basin (Fig. 1).

The Samana Suk Formation was studied in detail with regard to its sedimentology, paleontology and stratigraphy (Wadood et al., 2021a, b). The depositional environment for the rock unit was established in the Hazara area (Masood, 1989; Sheikh et al., 2001; Qureshi et al., 2008; Hussain et al., 2013). The depositional, diagenetic and sequence stratigraphic constraints on the reservoir quality of the unit in the Kala Chitta and western Salt ranges were documented in detail (Wadood et al., 2021a, b, 2021c). The paleoenvironments, paleoclimate, paleoenergy and paleosalinity for the Middle Jurassic in the Hazara region were established based on the sedimentological

investigation of the Samana Suk Formation (Saboor et al., 2020). The palynostratigraphy and reservoir potential of the Samana Suk Formation in the Kala Chitta Range were documented by Ahmad et al. (2020). The facies and geochemistry-based depositional environment and diagenetic evolution of the rock unit were determined in the Nizampur, Kala Chitta Range (Ullah Khan et al., 2020). The detailed literature review suggests that although the reservoir potential of the Samana Suk Formation has been determined for the Kala Chitta and Salt ranges of Pakistan, there are, however, high levels of spatial and temporal variability that exist in the petrophysical properties (porosity and permeability) of the carbonate rocks, duly resulting from both depositional and diagenetic processes. The current study is therefore aimed to generate a holistic understanding and therefore enable the prediction of the reservoir quality of the Samana Suk Formation in the Kohat Range, through integrating knowledge of the microfacies, sequence stratigraphy and diagenesis.

2 Geological Setting

In Pakistan, the Himalayas were formed as a result of the collision between the Indian and Karakoram plates during late Paleocene to early Eocene (Jadoon, 1992; Leech et al., 2005; Henderson et al., 2011; Wadood et al., 2021c). The Indus–Tsangpo suture marks the closure zone between the two plates in India and Tibet (Gansser, 1981), while in north Pakistan this suture branches off into the Main Karakoram Thrust (MKT) and the Main Mantle Thrust (Fig. 1; MMT; Powell and Conaghan, 1973; Tahirkheli, 1979; Rehman et al., 2011). The Kohistan Island Arc was formed due to intra-oceanic subduction during the Late Jurassic to Cretaceous (Le Fort, 1975; Jan and Asif, 1981; Windley, 1983; Chatterjee and Scotese, 2010; Rehman et al., 2011). The collision between India and the Kohistan Arc occurred along with the MMT during the Eocene (Tahirkheli, 1982; Khan et al., 2009; Chatterjee, 2013). A total of 500 km shortening of the Indian Plate was caused south of the MMT by underthrusting beneath the Kohistan Island Arc and the Karakoram Plate (Seeber et al., 1981; Ni and Barazangi, 1985) or by a widespread southward-directed thrust system and associated folding (crustal imbrications) over a broad zone (Molnar and Tapponier, 1975; Yeats and Lawrence, 1982; Molnar and Qidong, 1984; Coward and Butler, 1985; Bossart et al., 1988; Greco et al., 1989). After suturing at the MMT, the deformation front shifted southward to the hill ranges, which were uplifted and deformed along the Main Boundary Thrust (MBT) and the Salt Range Thrust (SRT) faults (Fig. 1; Yeats and Hussain, 1987). The MBT demarcates the southern limit of the Kohat, Samana, Margalla, Kala Chitta and Koh safed ranges. The MBT, which strikes east-west along most of the foreland basin, turns northwards, west of the Jhelum River, forming a major bend known as the Hazara Kashmir Syntaxis. It is a regional fault in north Pakistan that depicts the frontal region of the lesser Himalayan mountain range and brings the Mesozoic to Cenozoic rocks of Kohat, Kala Chitta and the Margalla hill ranges to

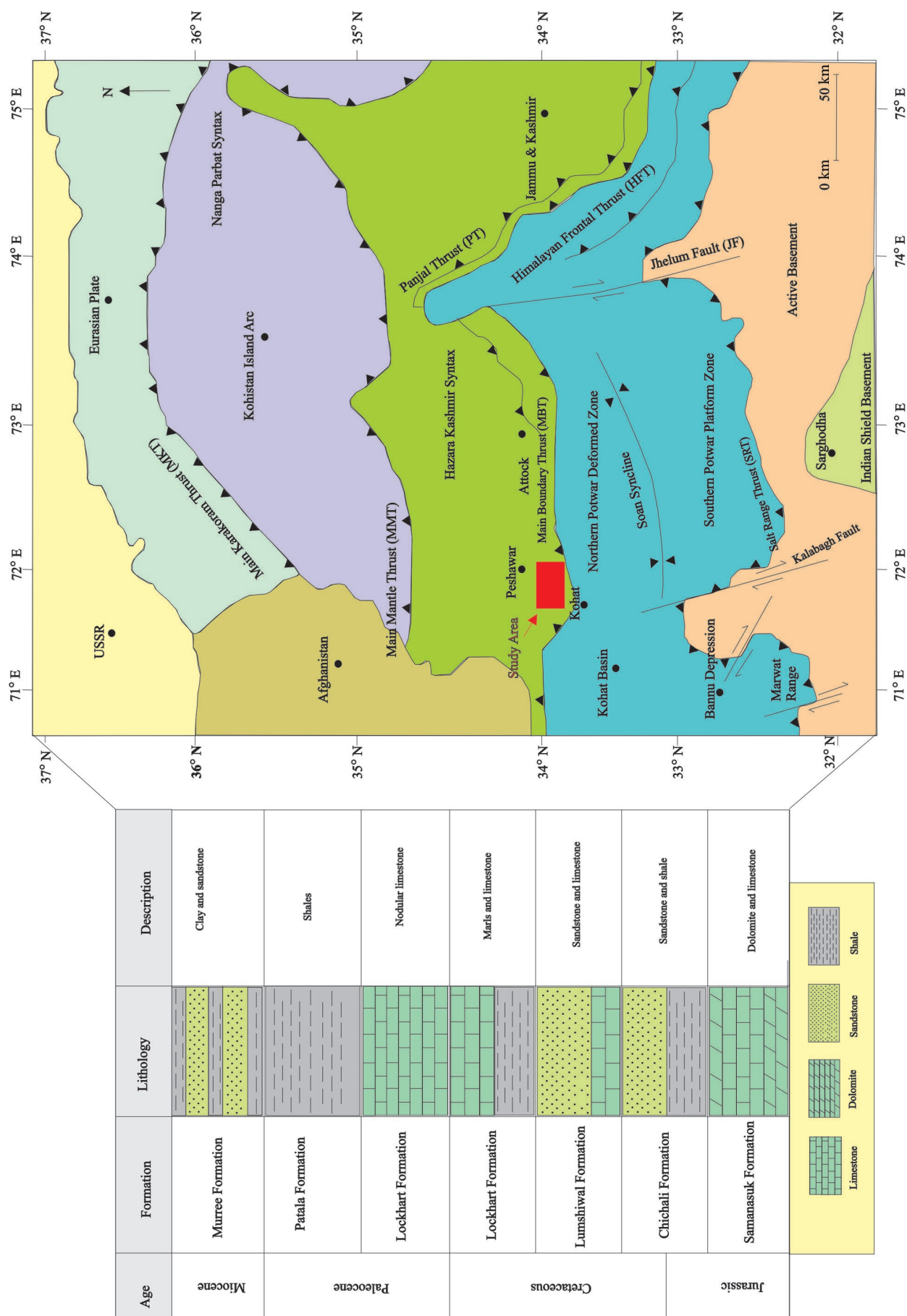


Fig. 1. Tectonic map of the study area near the Main Boundary Thrust (MBT), along with area stratigraphy where the rocks range from Jurassic to Miocene (modified after Kazmi & Rana, 1982; Shah, 2009).

the surface (Meissner et al., 1974; Khan et al., 1986). The study area is part of the Kohat Range, which is exposed along the MBT (Fig. 1). The rocks range in age from Jurassic to Miocene and are exposed in the study area (Fig. 1).

3 Materials and Methods

The Middle Jurassic Samana Suk Formation, which has an exposure of 227 m in the Kotal section of the Kohat Range, was logged and sampled in detail (Fig. 1). The outcrop description and features of the rock unit were recorded (Fig. 2). A total of 350 samples were collected from the section for petrographic and geochemical studies. Amongst these, 53 samples were stained with Alizarin Red-S and potassium ferricyanide solution, following Dickson (1965). The carbonate microfacies rocks were classified according to Dunham (1962). The depositional environments were established through integrating field investigations, sedimentary structures, textures, biota and compositions (see e.g., Wilson, 1975; Shinn, 1983a, b; Tucker and Wright, 1990; Flügel, 2010). The dolomite textures were described following the terminology and classification of Sibley and Gregg (1987) as well as other schemes, such as Friedman (1965), Shukla and Friedman (1983) and Mazzullo (1992), that were also taken into consideration. X-ray diffraction (XRD) was performed to identify the bulk mineralogy percentage composition of the selected samples. The diffraction of X-rays (Bragg's Law) is caused by the mineral phases when they reach a certain angle. The resultant chart from the diffractometer shows the X-ray diffraction pattern, which has a horizontal scale calibrated at 2 θ degree with the maximum intensity of the diffracted peaks being shown on the vertical axis. Minerals were identified by comparing the resulting peaks with the standard set of patterns compiled by the Joint Committee on Powder Diffraction Standards (JCPDS). The porosities and permeabilities were investigated by integrating the visual percentage estimation from thin sections imbued with blue epoxy resin and data taken from 3-centimeter diameter plugs using standard porosity-permeability measuring instrumentation under a net pressure of 1000 psi. The porosity types were quantified, based on image analysis of thin-sections with 300 point counts per thin-section. Data gained from the aforementioned sources were gathered to describe and define facies, diagenetic stages, as well as assess reservoir quality. The determined reservoir qualities (poor, moderate and good) correspond to certain porosity and permeability ranges. A composite figure comprising the vertical distribution of microfacies, field photographs, photomicrographs, depositional environments and sea-level curves was constructed (Fig. 3).

4 Results

4.1 Field observations

Detailed fieldwork was carried out in the Kotal section, Kohat Range, to observe and investigate important field features, as well as to collect samples for petrographic and geochemical analyses. For this latter purpose, samples

were collected at various intervals and occasionally from each bed, where lithological changes were observed. The formation is composed of a predominantly grayish limestone, alternating with rusty brown, grayish brown, dark gray to light grey dolostone beds (Fig. 2a). The Samana Suk Formation in the Kotal section is mainly composed of thick-bedded oolitic limestone. The ooid-rich beds have a thickness of 2–6 meters and are repeated at several intervals (Fig. 2b–d). In addition, there was a sharp contact between limestone and dolostone beds (Fig. 2e). Medium-bedded bioclastic limestone with parallel bedding was present. Various types of bioclasts of bivalve, brachiopod and skeletal grains were primarily observed at specific stratigraphic horizons (Fig. 2f–g). Bedding-parallel stylolites and calcite-filled fractures were found within this rock (Fig. 2h–i). The echinoderms (1–4 m) rich colonies were seen in association with the skeletal grains of gastropods and cephalopods (Fig. 2j). Thicker ooidal and peloidal-rich beds were observed in a repeating manner (Fig. 2k). In the studied section, different types of dolomite were identified. These dolomites were clearly distinguishable from limestone beds, based on a clear color contrast (Fig. 2l–m).

4.2 Microfacies analysis

Based on field data of bedding, lithology, sedimentary structure, texture, grain composition along with the fossil content in the thin-sections, sixteen microfacies were identified. The microfacies were assembled into three facies associations, allied to three depositional environments (peritidal, lagoonal and high-energy carbonate shoals). The microfacies analyses were mainly carried out by using the standard facies model for ramps by Flügel (2010). The overall characteristics and description of individual sedimentary facies as well as their facies associations, as recognized within the studied intervals, are given in Table 1.

4.2.1 Peritidal Flat Facies Association

(1) Bioclastic Peloidal Wackestone (MF1): The microfacies consists of peloids and bioclasts in a mud-supported texture (Fig. 4a). Peloids are mostly fecal pellets incorporated in this mud-supported texture. The bioclasts are disarticulated and non-abraded, comprising millioids, bivalve shells, sponge spicules and echinoderms. The bioturbation has turned the microfacies into having a patchy appearance. The predominantly mud-supported texture, together with extensive bioturbation with disarticulated and non-abraded bioclasts, indicate a low-energy shallow subtidal environment (Sattler et al., 2005). The association of peloids and fenestrae further restrict the facies to tidal flats (El-Sorogy et al., 2018). Based on the allochems, texture and biota, a peritidal setting is assigned to the facies (Fig. 5), which is correlated with RMF-16 of Flügel (2010).

(2) Fenestral Mudstone (MF2): A carbonate mud devoid of fossils and allochems is recorded for this facies with pervasive dolomite crystals. The light brownish dolomite crystals are coarse-grained, euhedral, homogeneous and non-ferroan (Fig. 4b). Rare silty quartz grains were observed. The hypersaline conditions restrict organic



Fig. 2. (a) Panoramic view of the study area in the Kotal section, Kohat Range; (b–d) limestone of the Samana Suk Formation showing ooids; (e) sharp contact between limestone and dolomite; (f–g) skeletal fragments of different bioclasts; (h–i) calcite veins and low to high amplitude stylolites indicated with an arrow in limestone beds; (j) skeletal grains of echinoderms, gastropods in grainstone facies; (k) peloids and ooid bed contact; (l) dolomite rock cross-cutting limestone bed; (m) contact between limestone and dolomite rock.

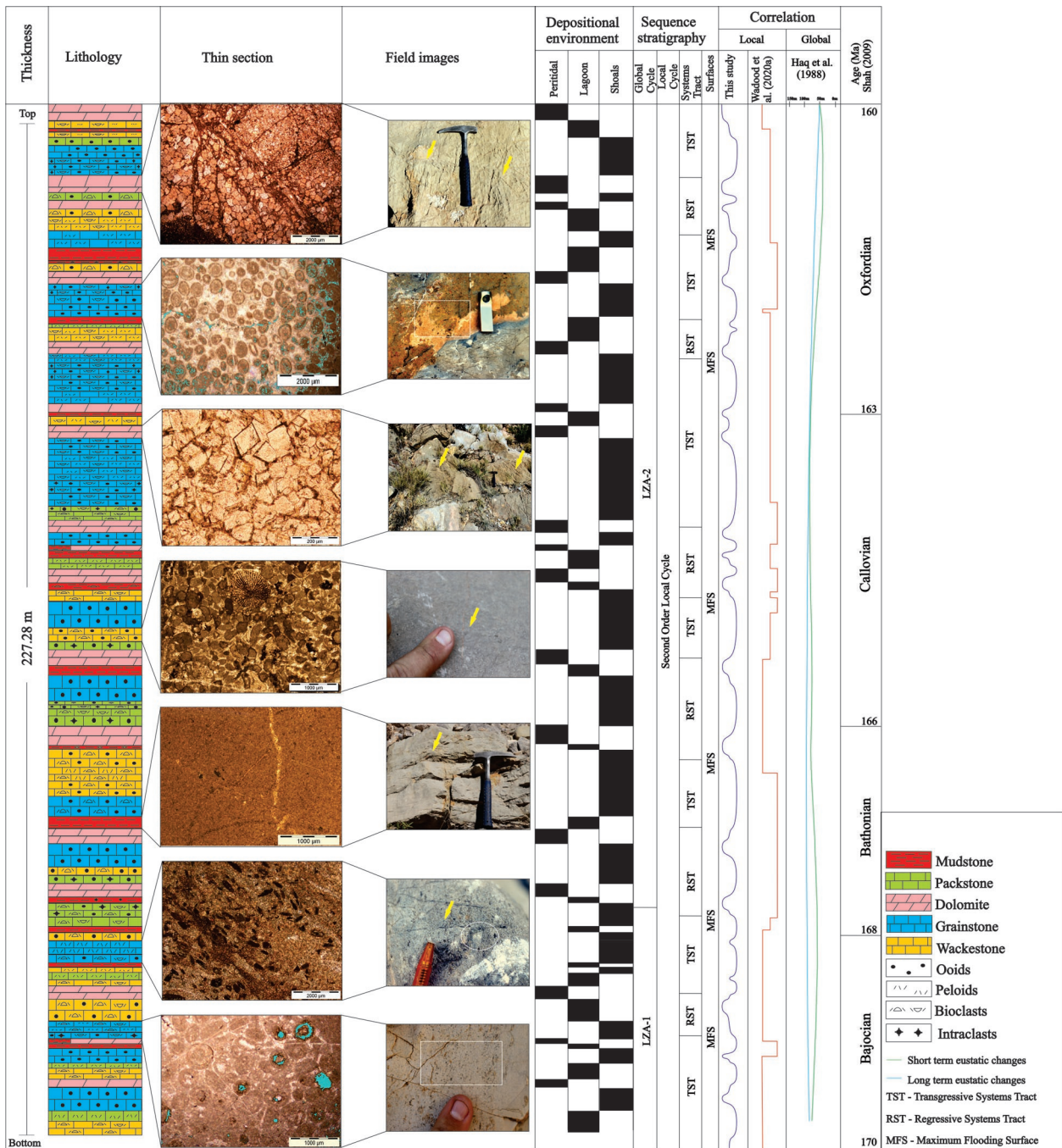


Fig. 3. Detailed log of the Samana Suk Formation, showing lithology, microfacies, depositional environments and sequence stratigraphy in the Kotal section of the Kohat Basin.

The inset view of the log shows the outcrop view and photomicrographs at various intervals.

activity within the peritidal setting, consequently leading to poor biodiversity (Fig. 5; Wanas, 2008; Karimi et al., 2015). The development of dolomite in mudstone under restricted conditions is attributed to a supratidal to upper intertidal environment (Shinn, 1983a). The facies is comparable to peritidal RMF-22 facies of Flügel (2010).

4.2.2 Lagoonal Facies Association

(1) Mudstone (MF3): The facies is dominated by carbonate mud with rare bioclasts and intraclasts (Fig. 4c).

Minor oval-shaped sparite grains and siliciclastic quartz were observed. The mudstone is non-laminated and homogeneous with a dense network of multiple calcite veins being visible. The dominant micritic matrix, massive texture, lack of open marine biota and bioturbation suggest that the facies is deposited in a low energy-restricted and hypersaline lagoon (Fig. 5; Nizami, 2008; Hussein et al., 2017). It is correlated with RMF-19 of Flügel (2010).

(2) Bioclastic Wackestone (MF4): The facies is characterized by the dominance of disarticulated and

Table 1 Overall summary of microfacies of the Jurassic Samana Suk Formation in the Kotal Section, Kohat Basin, Pakistan

Facies association	Microfacies code	Type	Sedimentary fabric	Main components	Depositional environment
Peritidal	MF-1	Bioclastic peloidal wackestone	Birdseye, extensive bioturbation	Peloids (25%–40%) and bioclasts (10%–20%) and predominantly mud	Low-energy and shallow subtidal environment: RMF-16
	MF-2	Intraclastic ooidal packstone	Lumpy structures, bioturbation, and lamination of ooids	Ooids (70%–80%), intraclasts (3%–5%)	Low-energy restricted supratidal and intertidal environment: RMF-24
	MF-3	Dolomudstone	Euhedral dolomite crystals, unfossiliferous, rare fenestral fabric and microbial filaments	Predominantly mudstone (70%–80%)	Warm and arid upper intertidal environment: RMF-22
Lagoon	MF-4	Mudstone	Non-laminated, homogeneous and black pebbles (as intraclasts)	Pure mudstone (about 90%)	Low-energy lagoonal environment: RMF-19
	MF-5	Bioclastic peloidal grainstone	Bioturbation and well-preserved fecal pellets	Peloids (65%–80%) and bioclasts (about 10%–15%)	Low-energy restricted lagoonal environment
	MF-6	Bioclastic wackestone	Non-apparent laminated and bioturbated due to micritization	Bioclast (about 30%–40%)	Brackish lagoonal with restricted circulation: RMF-17
	MF-7	Bioclastic mudstone	Rare dolomite rhombs, muddy matrix	Mud supported bioclast (about 40%–50%)	Restricted inner lagoon environment: RMF-19
	MF-8	Ooidal bioclastic wackestone	Micritized rims of ooids and bioclasts and well-sorted ooids	Bioclasts (40%–60%) and ooids (10%–15%)	Low-energy, restricted subtidal lagoonal environment: RMF-20
	MF-9	Peloidal packstone	Fecal pellets, micritized rims of peloids	Peloidal grains (about 80%–90%)	Semi-arid, hypersaline protected lagoonal environment
	MF-10	Bioclastic packstone	Micritized rims of bioclasts, microstylolites	Bioclasts (30%–40%)	Low-energy lagoonal setting: RMF-17
Carbonate sands and shoals	MF-11	Bioclastic intraclastic oolitic packstone	Slightly distinguishable lamination of ooids, micritized rims of ooids	(50%–70%) intraclasts (10%–25%) ooids	Moderate energy shoal environment
	MF-12	Bioclastic ooidal grainstone	Microbial encrusting, poorly-sorted and bioturbated	Ooids (50%–60%) and bioclasts (10%–15%)	Shallow water, restricted lagoonal to back-shoal environment: RMF-27
	MF-13	Bioclastic oolitic wackestone	Patchy appearance due to bioturbation and microstylolites	Ooids (30%–40%) and bioclasts (20%–30%)	Low-energy, partially restricted back shoal/bar: RMF-29
	MF-14	Intraclastic bioclastic ooidal grainstone	Partially micritized, cross-bedded, multi-laminar and tightly-packed pattern of ooids	Ooids (about 50%–70%), bioclasts (20%–30%) and intraclasts (10%–20%)	High-energy tidal bars and shoals: RMF-29
	MF-15	Ooidal grainstone	Multiple laminae of light and dark strips and well-sorted ooids	Ooids (80%–90%)	High-energy shoals, and bars, fair-weather wave base: RMF-29
	MF-16	Peloidal grainstone	Well-sorted, lack of micrite and rare microbial crusts	Peloids (80%–95%)	High-energy shoal depositional environment: RMF-29

fragmentary bioclasts, dispersed foraminifera, algae, and discernible shells such as ostracods, pelecypods, bivalves as well as echinoids (Fig. 4d). In addition, minor pellets and detrital quartz grains and peloids were also observed. The facies is mud-supported, with sporadic appearances of patchy dolomite being documented. The facies is both laminated and bioturbated. The presence of abundant matrix, low biodiversity and restricted fauna indicate deposition in a restricted low energy hypersaline lagoon (Fig. 5; Flügel, 2004; Hussain et al., 2013). The microfacies is correlated with the low diversity RMF-17 and the algal-rich bioclastic RMF-20 facies of Flügel (2010).

(3) Bioclastic Mudstone (MF5): The dominant allochems of the facies are bioclasts embedded in the micritic matrix. The bioclasts are comprised of foraminiferal shells, ostracods, molluscs and echinoids (Fig. 4e). Rare dolomite rhombs were also observed. The muddy matrix, restricted biota and fine silty quartz are

indicative of a low energy lagoon with a restricted circulation (Fig. 5; Rasser et al., 2005; Bachmann and Hirsch, 2006). The facies is similar to RMF-19 of Flügel (2010).

(4) Ooidal Bioclastic Wackestone (MF6): The allochems of the microfacies are predominantly bioclasts and ooids embedded in the carbonate matrix. The bioclasts include miliolids, ostracods, gastropods, brachiopods and green algae (Fig. 4f). The bioclasts and ooids are micritized and a rim is visible in both types of allochems. The restricted biota e.g. miliolids, green algae, gastropods, ostracods, as well as the micritized bioclasts and ooids, are suggestive of a restricted lagoonal environment with a slow rate of sedimentation (Fig. 5; Wilson, 1975; Hughes, 2009; Flügel, 2010). The facies correlates with RMF-20 of Flügel (2010).

(5) Peloidal Packstone (MF7): The dominant rounded fecal peloids with minute skeletal grains of bivalves and

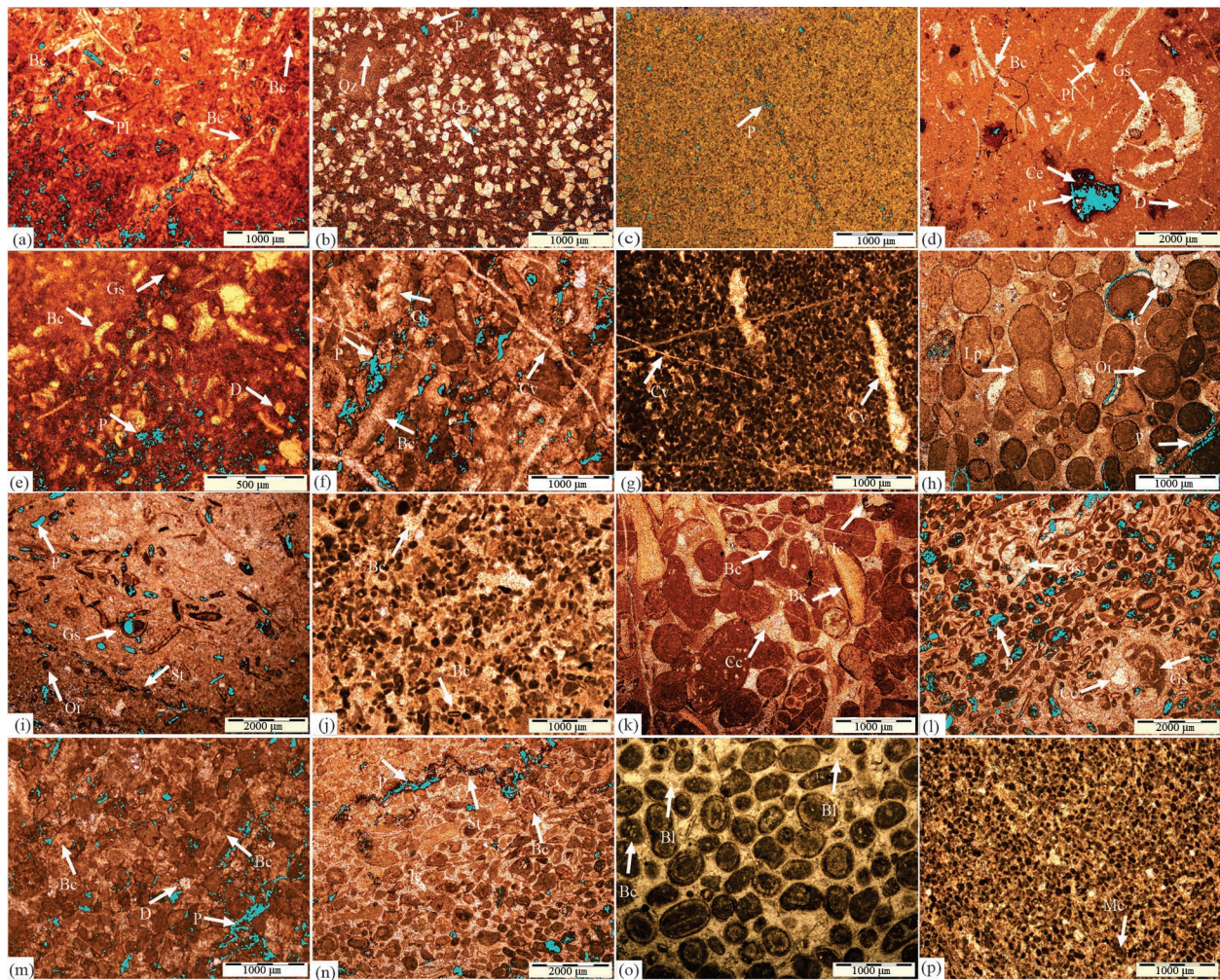


Fig. 4. (a) Bioclastic peloidal wackestone microfacies, with bioclasts, rare peloids and birdseye structure visible; (b) dolomudstone microfacies with rare quartz and porosity; (c) mudstone microfacies with porosity; (d) bioclastic wackestone having micrite envelopes in gastropods, along with bioclastic fragments, moldic porosity visible in cephalopod fragments and rare peloids; (e) bioclastic mudstone having gastropods, bioclasts and rare dolomite rhombs; (f) ooidal bioclastic wackestone, having gastropods and bioclasts with multiple calcite veins; (g) peloidal packstone, having rare bioclasts along with multiple calcite veins, blocky calcite cement can be seen occluding the pores; (h) intraclastic ooidal packstone, having intraclasts lumps and ooids; (i) bioclastic packstone microfacies, showing gastropods along with rare ooids and stylolites; (j) bioclastic peloidal grainstone with bioclasts; (k) bioclastic intraclastic ooidal packstone, with intraclasts, bioclasts and calcite cement; (l) bioclastic ooidal grainstone with skeletal remains of gastropods, where calcite cement is present in the center oomoldic porosity visible in ooids; (m) bioclastic oolitic wackestone, with bioclasts and rare ooids; (n) intraclastic bioclastic ooidal grainstone with bioclasts, intraclasts, stylolites exhibiting porosity in places; (o) ooidal grainstone with blocky calcite cement; (p) peloidal grainstone exhibiting rare micrite envelopes.

Blue color indicates porosity throughout. Bc–bioclast; Pl–peloids; Be–birdseye; P–porosity; Ic–intraclast; Lp–lumps; Oi–ooids; Qz–quartz; Gs–gastropods; Pl–peloids; D–dolomite; Cv–calcite veins; Bl–blocky calcite; Cc–calcite cement; Mc–micrite.

millioids as well as ooids are closely embedded in a carbonate matrix (Fig. 4g). Diagenesis has modified the facies by depositing intergranular and pore-filling blocky calcite cement. The micritization of the bioclasts, as well as the dense network of various calcite veins, are the outcome of diagenesis. The deposition of peloidal packstone is associated with shallow, low-energy, restricted lagoonal, shallow marine environments (Fig. 5; Flügel, 2010; Gischler et al., 2020).

4.2.3 Carbonate Shoal Facies Association

(1) Intraclastic Ooidal Packstone (MF8): The facies is

marked by a massive concentration of ooids with minor intraclasts and silty quartz. The ooids are very coarse-grained with a recognizable laminated fabric (Fig. 4h). The non-desiccated and non-abraded intraclasts were recorded without associated fenestral structures. Rare bioclasts and lumpy structures along with bioturbation and dissolution were observed. Intraclastic ooidal packstone and grainstone facies are deposited in a carbonate shoal environment (Flügel, 2004; Tavakoli and Jamalian, 2018). However, the grainstone textures represent high energy shoals, while packstone with embedded ooids and intraclasts argue for low energy leeward and seaward sides of the shoals (Fig. 5;

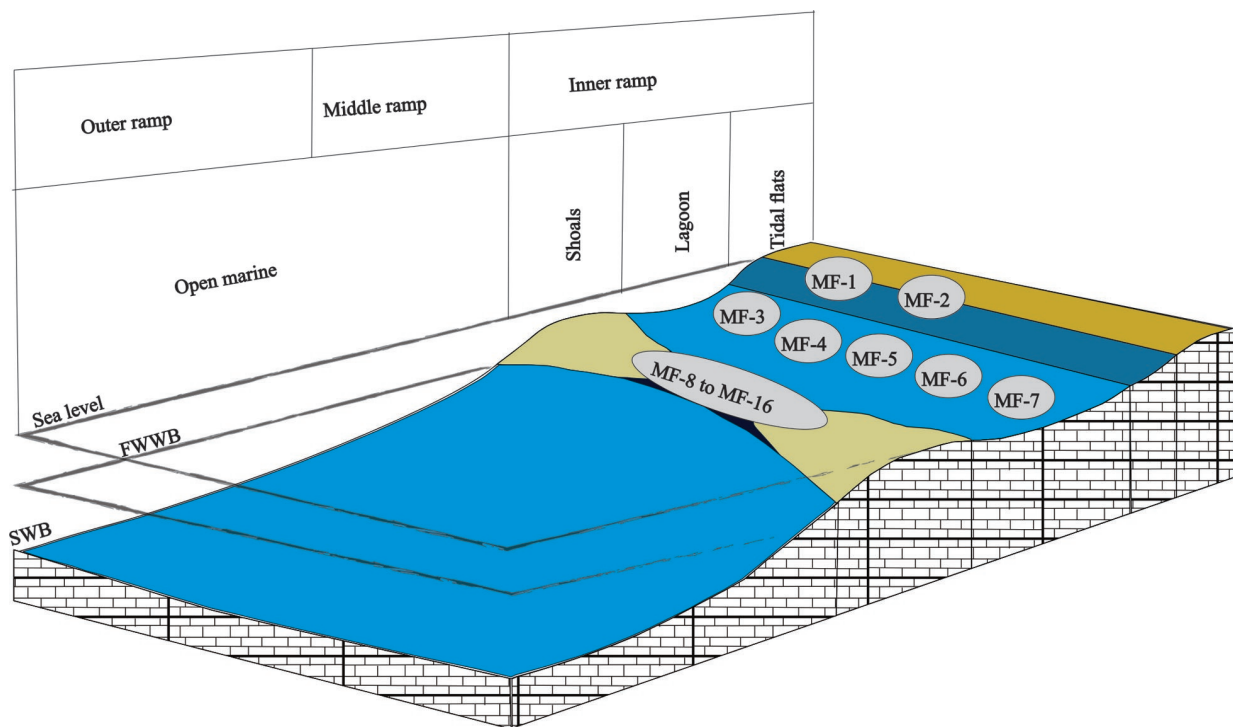


Fig. 5. Proposed depositional model for the Jurassic Samana Suk Formation.

FWWB = Fairweather wave base; MF-1 = Bioclastic peloidal wackestone; MF-2 = Fenestral mudstone; MF-3 = Mudstone; MF-4 = Bioclastic wackestone; MF-5 = Bioclastic mudstone; MF-6 = Ooidal bioclastic wackestone; MF-7 = Peloidal packstone; MF-8 = Intraclastic ooidal Packstone; MF-9 = Bioclastic packstone; MF-10 = Bioclastic peloidal grainstone; MF-11 = Bioclastic introclastic ooidal packstone; MF-12 = Bioclastic ooidal grainstone; MF-13 = Bioclastic oolitic wackestone; MF-14 = Intraclastic bioclastic ooidal grainstone; MF-15 = Ooidal grainstone; MF-16 = Peloidal grainstone.

Tavakoli and Jamalian, 2018). Thus, the facies is deposited on the low energy setting of carbonate shoals and correlates with RMF-14 of Flügel (2004).

(2) Bioclastic Packstone (MF9): The facies is marked by the dominance of bioclasts embedded in the carbonate matrix (Fig. 4i). The bioclasts include echinoderms, ostracods, foraminifera, sponge spicules, gastropods and brachiopods. Micritization of bioclasts and stylolitization were observed. The grain-supported texture with carbonate mud in the pore spaces suggests deposition at the interface of a high-energy inner shelf and a low-energy middle ramp and is correlated with RMF-14 (Fig. 5; Flügel, 2010).

(3) Bioclastic Peloidal Grainstone (MF10): In this microfacies, abundant peloids of fecal origin with significant bioclasts are glued together by sparry cement (Fig. 4j). The coarser bioclasts are composed of bivalves, gastropods and rare echinoids, while the smaller benthic foraminifera constitute the finer fraction. Bioturbation and extensive micritization are common in this microfacies. The peloids are formed as a result of micritization of carbonate grains by endolithic algae in low-energy, restricted and shallow water environments (Hussain et al., 2013). Likewise, due to the fragility of the pellets, these cannot withstand high-energy settings, indicating a low-energy setting. Based on the types of allochems, as well as a scarcity of biota in association with benthic foraminifera, bivalves and gastropods suggest deposition in a shoal setting with quick cementation, to avoid the abrasion of fragile allochems (Fig. 5; Tucker and Wright, 2009).

(4) Bioclastic Intraclastic Ooidal Packstone (MF11): This microfacies is dominated by ooids, followed by intraclasts and bioclasts. The ooids are very coarse-grained with visible internal lamination (Fig. 4k). The bioclasts fraction is dominated by pelecypods and gastropods, in association with minor occurrences of echinoid and serpulid colonies. The internal fabric of the allochems is well-preserved, due to poor micritization. The ooids are usually formed on the platform margin, in high energy conditions. Serpulid colonies thrive in shallow warm water (Wilson, 1975). The minor fraction of carbonate mud, with diverse marine bioclasts and intraclasts, suggest deposition in a higher energy setting (Flügel, 2010). Based on the dominant photozoans, such as ooids and associated allochems, inner ramp shoal settings are attributed to the deposition of this microfacies (Fig. 5).

(5) Bioclastic Ooidal Grainstone (MF12): The facies is dominated by photozoan ooids, in association with a significant amount of bioclasts, such as gastropods and echinoderms. The allochems are glued together by sparry cement. Minor elongated peloids and indeterminate fossil shells were seen (Fig. 4l). Ooids are usually deposited on the platform margin under high-energy conditions (Gischler et al., 2020). The grainstone texture and lack of bioturbation further support such an environmental interpretation (Heerwagen and Martini, 2020). The rounded to sub-rounded ooids with some shell fragments and elongated peloids indicate carbonate shoal settings (Husseini et al., 2017). Based on the dominance of photozoans and the cemented texture, an inner ramp

shoal setting is assigned to the deposition of this facies (Fig. 5). The facies correlates well with RMF-27 of Flügel (2010).

(6) Bioclastic Oolitic Wackestone (MF13): The ooids dominating the facies are duly succeeded by bioclasts in abundance. The cortices of ooids are rounded to sub-rounded and micritized (Fig. 4m). The internal laminations of ooids are slightly visible and their nuclei are comprised of older ooids. The partially discernible bioclasts consist of pelecypods and echinoids. Minor occurrences of rare peloids, sponge spicules and smaller benthic foraminifera were observed. Dolomite rhombs were observed in places. The high degree of bioturbation, presence of ooids in the micritic matrix showing textural inversion and scarce fauna overall indicate a low-energy, partially restricted, shallow subtidal environment, probably in the back shoal/bar area (Fig. 5; Flügel, 2010).

(7) Intraclastic Bioclastic Ooidal Grainstone (MF14): The ooids, bioclasts and intraclasts constitute their respective abundances in the grainstone texture of the facies. The well-developed ooids are tightly packed and have preserved multiple concentric laminae in their cortices (Fig. 4n), while the nuclei are mostly peloids and bioclasts with calcite-filled fractures. The well-sorted, tightly-packed and cross-bedded ooids indicates high energy settings above the wave base e.g. beaches, tidal bars and shoals (Flügel, 2010). Furthermore, the concentric cortices of the ooids characterize a high-energy depositional environment (Loreau and Purser, 1973; Harris, 1979). Based on the types of allochems, cement and sedimentary structures, an inner carbonate ramp environment is proposed as the environment for the deposition of this facies (Fig. 5). The microfacies is similar to RMF-29 of Flügel (2010).

(8) Ooidal Grainstone (MF15): The facies is marked by well-rounded ooidal grains that have recorded multiple alternating dark and light layers in their cortices, while their nuclei are predominantly composed of laminar peloids, older ooids and fragments of bioclasts (Fig. 4o). The facies cement is micro-sparite, while in places a coarse blocky calcite cement, probably of diagenetic origin, is also present. The well-sorted and concentric coarser ooids in the grainstone are indicative of a high-energy setting above the wave (Reolid et al., 2007). The high-energy deposits are characteristically

associated with shoal and bar environments, either on or near the seaward side of carbonate platforms (Wilson, 1975; Van Buchem et al., 2002; Flügel, 2010). Based on the abundances of ooids, the paucity of micrite and the well-sorted nature of the grains, a shoal environment of high-energy above a fair-weather wave base is suggested for the facies (Insalaco et al., 2006; Hashmie et al., 2016; Fig. 5). The facies correlates with RMF-29 of Flügel (2010).

(9) Peloidal Grainstone (MF16): The facies almost exclusively consists of well-sorted peloids, glued together by sparry calcite cement (Fig. 4p). The presence of sparry cement, well-sorted grains and a lack of micrite all indicate a high-energy shoal depositional environment (Flügel, 2010). The carbonate shoal environment is considered to have high wave energy and relatively low tidal energy, with minimal associated mud (Lasemi et al., 2012). The abundance of peloids and rare ooids suggests deposition in high-energy settings (Ham, 1962; Powell, 1979; Kadri, 1995; Scholle and Ulmer-Scholle, 2003). The peloid grains may deposit in those shoals which are characterized by low circulation, warm and shallow water depth (Jank et al., 2006) and hence these cannot withstand a high-energy environment. The well-preserved peloid grains thus indicate rapid cementation in the shoal setting (Fig. 5). This microfacies is compatible with RMF-29 of Flügel (2010).

4.3 Porosity and permeability

The porosities of the microfacies were investigated using outcrop, petrography and plug porosity, while permeability analyses were carried out using plug permeability (Figs. 2, 4, 6, 7). At the outcrop, the Samana Suk Formation has highly fractured limestone and dolomite units (Fig. 2m). The fractures range from small and hairline to large and open. The dolomitic unit is more fractured, compared to the limestone unit, which has ultimately enhanced the reservoir properties. Stylolites of low to high amplitudes were also observed (Fig. 2i). The petrography revealed various types of micro-porosities, i.e. moldic, fracture, inter-particle, intraparticle and vuggy (Figs. 4, 7). Porosity is also observed along the dolomite grains (Fig. 7l-n). Measurements of plugs revealed a wide range of porosity values, ranging from 0.87%–6.13%, while the permeability ranged from 0.21–3.11 millidarcy (Fig. 6). The integration of petrography and plug data

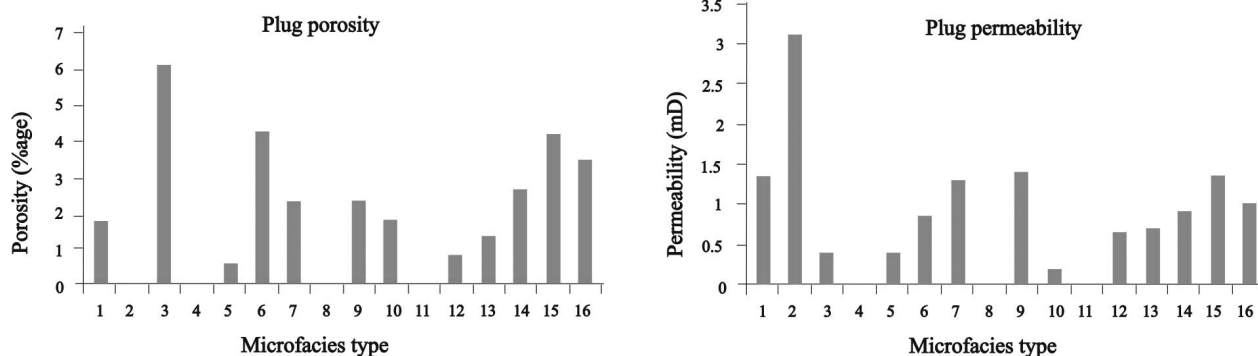


Fig. 6. Plug porosity/permeability results of the selected rock samples from each microfacies of the Jurassic Samana Suk Formation.

indicate higher values of porosities in carbonate shoal facies, while moderate to poor values of porosities are reported from lagoonal and peritidal facies, respectively (Table 2).

4.4 Diagenesis

The diagenesis of the Samana Suk Formation was elucidated using basic petrography, complemented by the outcrop data. The petrography identified different diagenetic processes, such as compaction, cementation, micritization, dissolution and dolomitization (Fig. 7). The diagenetic processes proved crucial for establishing the diagenetic environment, paragenetic sequence and reservoir potential of the shallow marine carbonates of the Samana Suk Formation. The details of various diagenetic processes recorded within the studied unit are given below.

4.4.1 Fracturing

Various small to large scale fractures were observed within the Samana Suk Formation (Fig. 7a). The orientation of such fractures varied from bedding-parallel, oblique to perpendicular. The fractures were seen both at the outcrop and within the thin-section. The polyphase fractures were formed both in early-stage diagenesis due to burial and in the late telogenetic stage, as a result of tectonic stresses and loading.

4.4.2 Compaction

The Samana Suk Formation has undergone anomalous shallow to deep burial compaction as a result of overlying deposition. The mechanical compaction as a result of strain concentration at grain contacts has caused broken deformed grains and sutured contacts between grains (Fig. 7b). The deep burial has enhanced pressure solution and as a result the sutured contacts are laterally joined together to constitute continuous stylolites (Fig. 7c–d).

4.4.3 Cementation

In the Samana Suk Formation, cementation can be seen in the form of calcite veins and patches in limestone and dolostone units (Fig. 7e–f). These cements have partially to completely filled fractures and pore spaces. The different types of cement identified are granular equant, elongated blocky, syntaxial overgrowth crystals, isopachous fibrous and dogtooth calcite. The granular equant calcite cement comprises subhedral to anhedral crystals formed in intergranular spaces, as well as in fractures (Fig. 7g). Blocky calcite cement is mainly developed in shoal-related facies and consists of moderate to coarse-grained calcite crystals that usually occur in intergranular spaces (Fig. 7h). In marine phreatic conditions, syntaxial overgrowth cement formed more rapidly and surrounds the grains. In some grainstone facies, the syntaxial overgrowth cement alone is present (Fig. 7i). Dogtooth cement is rarely present in the Samana Suk Formation. This cement postdates the formation of blocky calcite cement (Fig. 7j).

4.4.4 Micritization

Depending upon the water depth and rate of sedimentation, the micritization of grains varies. It is most commonly developed along the rims of ooids and bioclasts (Fig. 7k). The micritization can be either constructive or destructive (Flügel, 2010). Destructive micritization occurred as a result of repeated boring and subsequent infilling of the bores with micrite. Constructive micritization usually formed as a result of accretion of calcified filamentous algae on the surface of the grains. In the Samana Suk Formation, both constructive and destructive micritization was observed. Micritization is a common process that usually occurs in shallow marine environments and is caused by several different micro-organisms, such as endolithic algae and fungi (Reid and MacIntyre, 2000; Beigi et al., 2017).

Table 2 Details of the petrographic and plug porosity and permeability results, along with diagenetic alterations that affected the depositional porosity of the Jurassic Samana Suk Formation

Microfacies	Diagenetic alteration	Porosity type	Reservoir quality	Porosity (%)	Permeability (md)
MF-1	Micritization & bioturbation	Channel, Boring	Poor	1.83	1.36
MF-2	Bioturbation, secondary dissolution	Boring	Poor	Sample too tight	3.11
MF-3	Neomorphism: dolosparite recrystallization to dolomicrite	Very rare, Fenestral	Good	6.13	0.41
MF-4	Micritization and compaction	Fenestral & Intercrystal	Poor	Sample too tight	
MF-5	Micritization, bioturbation compaction, cementation by blocky cement	Shelter	Poor	0.63	0.41
MF-6	Bioturbation and subsequent extensive micritization	Burrow & Fenestral	Moderate	4.27	0.87
MF-7	Bioturbation, micritization & dissolution	Boring & Fenestral	Good	2.38	1.3
MF-8	Neomorphism, micritization, multiple set of veins, dissolution	Interparticle & Moldic	Poor	Sample too tight	
MF-9	Micritization, vug-filling, cementation by blocky calcite, multiple set of veins & dissolution	Interparticle	Good	2.36	1.41
MF-10	Micrite envelopes, grain penetration (compaction), cementation by sparry calcite and fracture filling (late calcite veins)	Intraparticle & Vuggy	Moderate	1.87	0.21
MF-11	Partial micritization, strong dissolution & neomorphism by sparry calcite	Interparticle and Intraparticle	Poor	Sample too tight	
MF-12	Bioturbation, micritization, compaction, dissolution & late stage calcite veins	Vuggy	Poor	0.87	0.66
MF-13	Partial micritization, chemical compaction & late-stage calcite veins	Intraparticle	Moderate	1.41	0.7
MF-14	Physical compaction & cementation by blocky cement	Interparticle	Good	2.71	0.93
MF-15	Minor dissolution, neomorphism and voids filled by sparry calcite	Rare Moldic & Shelter	Good	4.17	1.37
MF-16	Micritization, compaction & neomorphism	Intraparticle and Shelter	Good	3.5	1.03

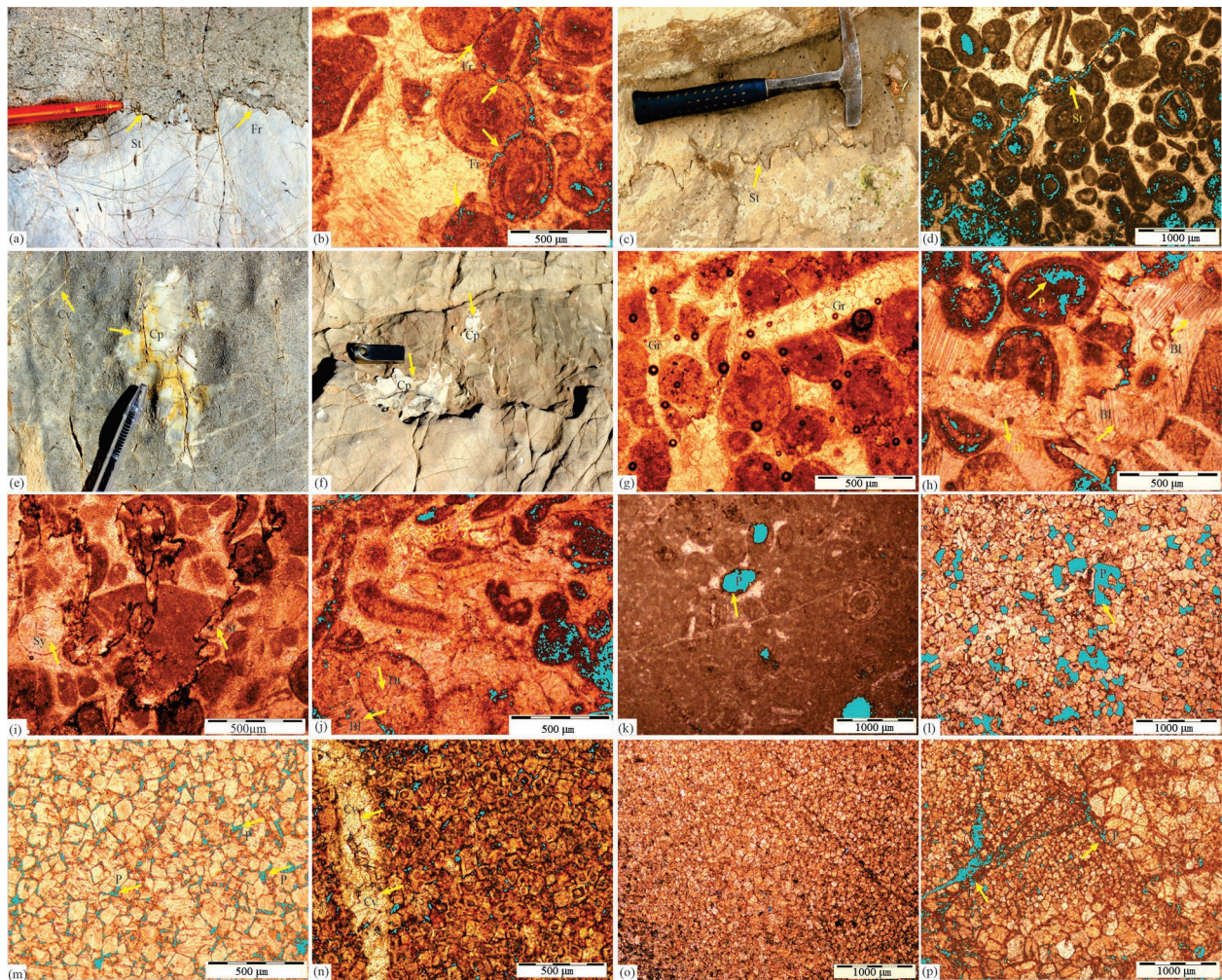


Fig. 7. (a) Field photograph showing mechanical and chemical compaction, with stylolites formed by chemical compaction; (b) photomicrograph showing deformed grains and sutured contacts producing fractures in ooids; (c) field photograph showing stylolites; (d) photomicrograph showing stylolites and porosity; (e) calcite cement present in the form of patches and vein-filling in limestone; (f) calcite in the form of a patch in dolomite; (g) granular equant calcite cement in vein-filling; (h) blocky calcite cement present between intergranular spaces; (i) syntaxial overgrowth cement in ooids along with stylolite and porosity in blue color; (j) dogtooth cement showing sharp edges along with blocky cement and porosity; (k) micritization of ooids, along with oomoldic porosity in blue color; (l) dissolution in dolomite creating porosity in blue color; (m) coarse-grained euhedral dolomite showing intercrystalline porosity; (n) coarse-grained euhedral zoned dolomite along with calcite vein; (o) fine-grained subhedral dolomite; (p) coarse-grained subhedral to anhedral dolomite, along with fine-grained subhedral dolomite.

Blue color shows porosity throughout. Fr—fractures; P—porosity; St—stylolites; Cp—calcite patches; Cv—calcite vein; Gr—granular cement; Sy—syntaxial overgrowth cement; Bl—blocky cement; Dt—dogtooth cement.

4.4.5 Dissolution

Dissolution is a secondary process, as a result of which different types of porosity have been developed in the Samana Suk Formation, i.e. intragranular, intergranular, moldic vuggy and fracture porosity. Due to dissolution, vuggy porosity is evident in dolomite but rarely seen in fenestral mudstone facies (Fig. 7l).

4.4.6 Dolomitization

In the Samana Suk Formation, diagenetically different types of dolomites were identified (Fig. 7l–p) such as (1) coarse-grained euhedral dolomite; (2) coarse-grained euhedral zoned dolomite; (3) fine-grained subhedral dolomite; (4) coarse-grained subhedral to anhedral

dolomite. Coarse-grained euhedral dolomite consists of coarse dolomite rhombs with well-developed crystal boundaries. The dolomite crystals observed range in size from 50–100 μm . These are early-formed dolomite crystals that replaced the matrix and grains of the precursor rock. This type of dolomite has an intergranular and vuggy porosity (Fig. 7m). Coarse-grained euhedral zoned dolomite is formed from the earlier formed dolomite. These dolomite rhombs are tightly packed and range in size from 60–110 μm . Calcite veins cross-cut this dolomite (Fig. 7n).

4.5 Mineralogical studies

To determine the bulk mineralogy of the rocks, sharp

diffraction peaks were obtained for different samples of limestone and dolomite using X-Ray diffraction (XRD) analyses (Fig. 8). The samples were selected from dolostone, grainstone and mudstone. The samples from wackestone were avoided because it falls in the middle of mudstone and grainstone, so XRD data would not be of any assistance in giving crucial information about the effect of impurities on the reservoir potential of the facies. The XRD data of the limestone revealed that the ooidal

grains show the dominance of calcite in close association with pyrite, quartz and cinnabar, while the XRD analyses of the mudstone facies revealed the dominance of the calcite phase, in association with pyrite and other forms of silica.

5 Discussion

5.1 Depositional model

The high-resolution microfacies analysis has revealed the detailed ramp environment for the Samana Suk Formation. The sub-environments within the ramp range from low energy peritidal and lagoonal to a high energy shoal setting in a quasi-periodic manner (Fig. 5). The proximal lagoon to distal peritidal carbonates are characterized by mudstone and wackestone microfacies. The restricted circulations amongst these facies are marked by the dominance of restricted hypersaline fauna and subdued open marine biota, while the low energy conditions are marked by pelletization, abundant carbonate mud, bioturbation and preservation of laminated fabric in places. The carbonate shoals are represented by packstone and grainstone microfacies. Such facies are characterized by both heterozoan and photozoan-dominated carbonates. The heterozoan skeletal-rich facies shows a strong affinity with open marine saline conditions, while the photozoan carbonates are dominated by non-skeletal carbonates. The high energy conditions of the carbonate shoals are indicated by ooids, grain-supported texture, heavy cementation, intraclasts and absence of bioturbation. The open marine saline conditions are indicated by bioclasts and photozoans such as ooids. The Samana Suk Formation is characterized by the dominance of carbonate shoal facies which exceed 50% of the total rock, followed by lagoonal and peritidal facies respectively (Fig. 3). The shoal facies are interspersed throughout the stratigraphic thickness of the unit and are separated by lagoonal/peritidal facies. The spatial distribution of similar microfacies within the Samana Suk Formation are recorded in the Upper Indus Basin (Ahmad et al., 2020; Saboor et al., 2020; Ullah Khan et al., 2020; Wadood et al., 2021a–c). The absence of the Samanasuk facies in Eastern and Central Potwar, its subdued nature in the western Salt Range and its expanded thickness in the Kohat and Hazara regions suggest that the shoreline of the ramp was located in a northeast-southwest oriented basin that was deepening to the north and west in the region (Saboor et al., 2020). The exposure of the synchronous shoals to peritidal facies of the Chiltan Formation in the Badin and Jacobabad areas and their expanded thickness in the Sulaiman and Kirthar ranges (Kadri, 1995; Shah, 2009) suggest the extension of the ramp into the Lower Indus Basin. The Middle Jurassic carbonates are widely distributed in the adjacent continents e.g. India, Southern UAE, Central Oman, Central Saudi Arabia and the Central High Atlas of Morocco (Rousseau et al., 2005; Addi and Chafiki, 2013; Hollis et al., 2017; Yousif et al., 2018; Ahmad et al., 2020). Such Middle Jurassic shallow carbonates are reflected at this time in their widespread deposition in various parts of the globe, e.g. Portugal, England,

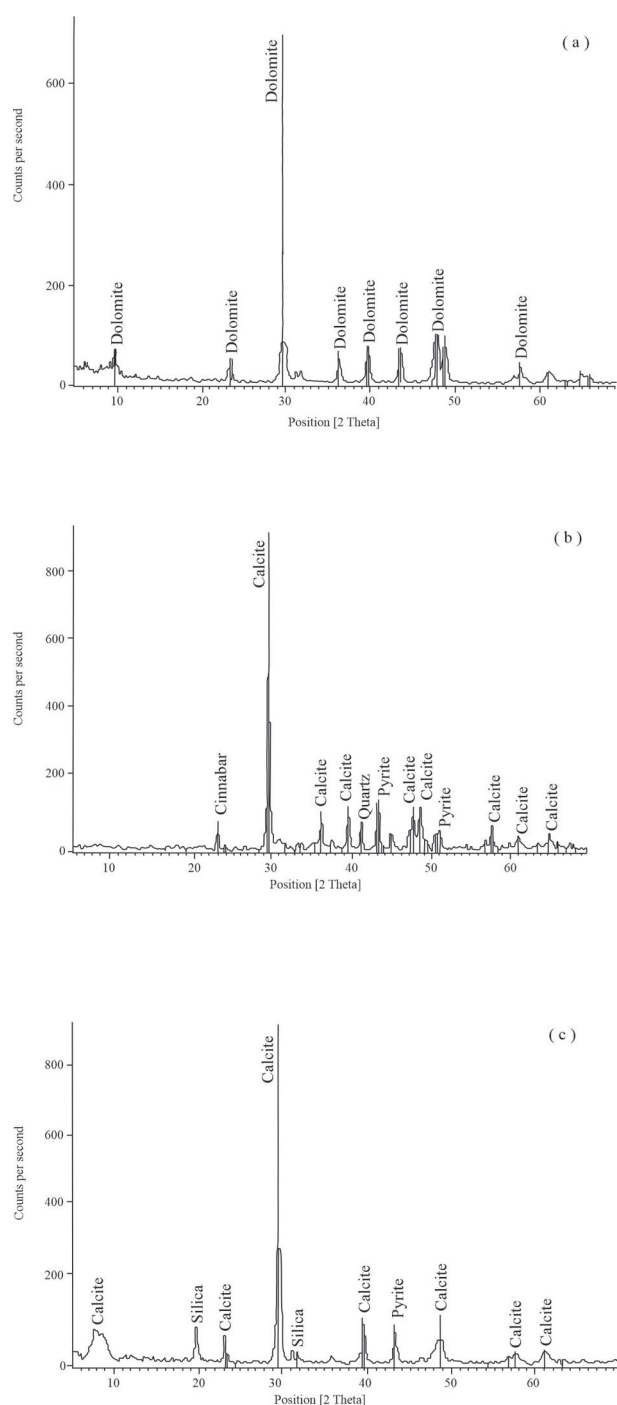


Fig. 8. X-ray diffraction peaks of the minerals in the Samana Suk Formation.

(a) Dolomite rock minerals; (b–c) limestone rock minerals.

Switzerland and Turkey (Sellwood et al., 1985; Ayyıldız et al., 2001; Brigaud et al., 2009; Lazăr et al., 2013; Wetzel et al., 2013; Azerêdo et al., 2020).

5.2 Sequence stratigraphy

The advent of sequence stratigraphy and its application to the geometry and evolution of carbonate platforms in response to sea-level fluctuations and accommodation space has gained momentum in recent years (Sarg, 1988; Schlager, 1992; Handford and Loucks, 1993). Sequence stratigraphy is a widely used tool within the hydrocarbon industry, to better comprehend the sedimentary geometries, controls on basin filling and diagenetic evolution of carbonates, as well as in the accurate demarcation of hydrocarbon reservoirs (Booler and Tucker, 2002). Carbonate sediments are sensitive to sea-level changes (Morad et al., 2012). A slight change in sea level causes a change in carbonate grains, matrix/cement and the exposure time of grains to ocean chemistry (Tucker and Wright, 2009; Morad et al., 2012). Therefore, the character of the carbonate facies can be used for precise interpretation of paleoenvironments (Flügel, 2010). In the present study, the sea-level curve for the Samana Suk Formation in the Kohat Basin was reconstructed using detailed microfacies (Fig. 3). The rock unit is deposited over a span of 10 Ma (see e.g. Shah, 2009). In order to establish a chronostratigraphic framework for the Samana Suk Formation, the 10 Ma interval was divided into equal time slices, assuming that the rate of sedimentation was uniform (Fig. 3). The Samana Suk Formation was deposited in one 2nd order cycle and has in its turn recorded multiple 3rd order transgressive and regressive cycles, according to Embry and Johannessen (2017). The 2nd order cycle can be correlated with LZA-1 and LZA-2 of Haq et al. (1988). Based on the microfacies-based paleoenvironments, a total of seven Transgressive Systems Tracts (TSTs) and six Regressive Systems Tracts (RSTs) have been documented (Fig. 3). The TSTs and RSTs alternate in vertical section and are predominantly uniform in their thicknesses. However, individual TSTs are relatively thicker when compared to RSTs, while the overall thickness of TST strata is greater than its RST counterpart, hence the transgressive episodes and overall sea-level rise last longer than in regression. The TSTs are predominantly comprised of grainstone and packstone microfacies, while the RSTs are dominated by wackestone and mudstone facies.

The sea-level curve generated from the interpretation of microfacies was correlated with the local sea-level curve of the Samana Suk Formation in the Kala Chitta Range (see Wadood et al., 2021a) and the global sea-level curve of Haq et al. (1988). The correlation of the relative sea-level curve of the present study with the global sea-level curve shows a complete mismatch during the Bathonian-Bajocian, however a consistent transgressive trend is recorded both locally and globally during the Callovian (Fig. 3). The mismatch between the relative sea-level curve of the Samana Suk Formation and the global curve is also observed during the Oxfordian. A predominant match exists between the sea-level curves of the Samana

Suk Formation in the study area and at Kala Chitta (Wadood et al., 2021a), however, high-frequency sea-level fluctuations were observed within the former. The basis for such high-frequency fluctuations is thought to be due to the expanded thickness and high sample resolution in the study area. The sea-level fluctuations are recorded in excess of a meter, with greater variations in thickness, hence episodic tectonicity has caused such fluctuations instead of the cycles of Milanković (Spence and Tucker, 2007). Tectonic control is further confirmed by the non-systematic cyclic stacking pattern, thickness trends and irregular variation in cycle types (Bosence et al., 2009). The variations in types and thickness of the facies cycles have resulted from the continuous, abrupt and episodic tectonic pulses.

5.3 Paragenetic sequence of the Samana Suk Formation

A detailed paragenetic sequence has been established for the Jurassic Samana Suk Formation, based on various diagenetic features (Fig. 9). The early stage of diagenesis that extensively altered the primary depositional structures included micritization. This event indicates a longer exposure time of the sediments to microbial activity in the marine phreatic environment (Bathurst, 1983; Flügel, 2010). Besides the formation of the micritic envelopes, other marine diagenetic events include early mechanical and chemical compaction, followed by the cementation of sediments by granular, blocky, isopachous fibrous calcite cement, that are all indicative of early marine diagenesis. The granular and blocky cementation occurred in two stages: (1) in this stage, the cement was precipitated in the pore spaces of the carbonate grains; (2) the cement also precipitated in the voids as a second generation. The mechanical compaction as a result of overburden pressure caused the formation of fractures both at the outcrop as well as at microscopic levels. The chemical compaction due to burial has produced low to high amplitude stylolites at various stratigraphic heights. The burial has also caused the formation of zoned dolomite (Guo et al., 2016). Similar dolomite of burial origin has been reported globally (Drivet and Mountjoy, 1997; Al-Aasm and Packard, 2000; Chen et al., 2004; Azmy et al., 2009; Conliffe et al., 2012; Rott and Qing, 2013). Fine-grained subhedral dolomite crystals range in size from 20–30 μm . The dolomite crystals are tightly packed together (Fig. 7o). These dolomites were formed by the compactional dewatering of the dolomitizing fluids from deep basinal siliciclastics, along with the E–W trending MBT (Khan et al., 2021). Coarse-grained subhedral to anhedral dolomites are tightly packed where multiple fractures cross-cut these dolomites. The crystal size of this dolomite ranges from 300–500 μm . It can be seen that these dolomites cross-cut the earlier formed fine-grained dolomite (Fig. 7p). The coarsening crystals are likely to result from crystal overgrowth. In these dolomites, crystals are coarser in size, more curved and tightly-packed, indicating more rapid growth at higher temperatures (Montañez and Read, 1992; Al-Aasm and Packard, 2000). The mechanical and chemical

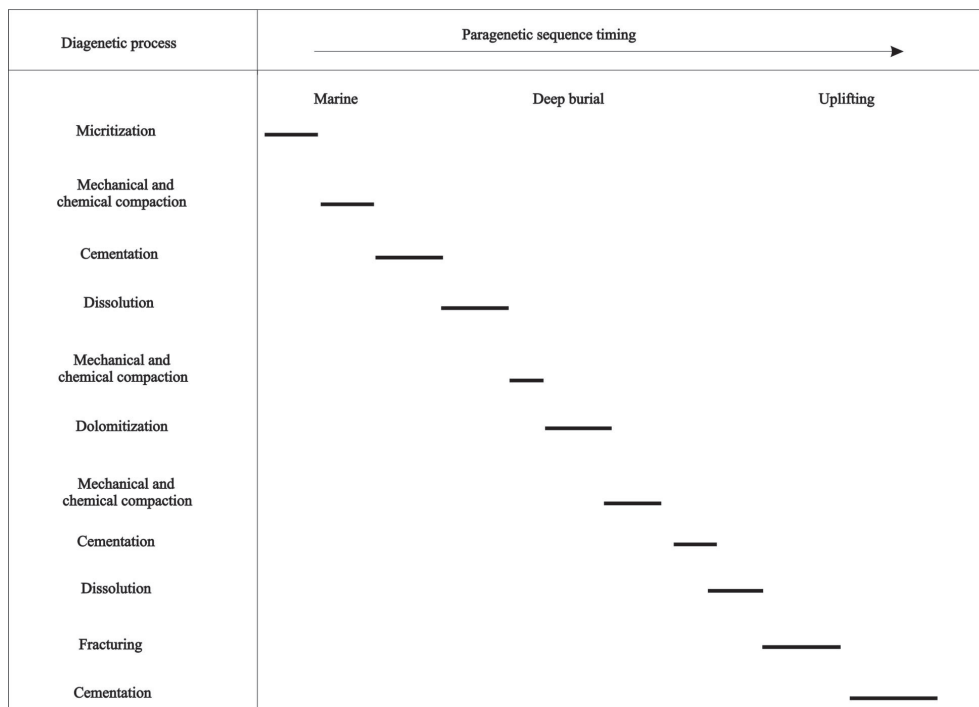


Fig. 9. Proposed paragenetic sequence of the Jurassic Samana Suk Formation.

compaction occurred during shallow and deep burial. Under meteoric phreatic conditions, dissolution of carbonate grains, particularly bioclastic fragments, have significantly influenced the reservoir behavior of the carbonate succession. The inflow of freshwater resulted in the dissolution of carbonate grains. The process of dolomitization occurred in several phases, which are evident in the differences in the texture of the dolomite crystals, as well as the cross-cutting relationship amongst the dolomite crystals (Fig. 7p). Late-stage, deep burial fractures led Mg-rich fluids through the rock fabric, causing dolomitization, generating intercrystalline porosity. In the later stages, multiple uplifting events, as suggested by the tectonic setting of the area (Tahirkheli et al., 1979; Rehman et al., 2011), caused multiple fracturing and cementation phases, which overgrew the previous features.

5.4 Depositional and diagenetic controls on the reservoir quality

In the study area, the spatial distribution and stacking pattern of depositional facies and diagenesis have greatly influenced reservoir geometry and reservoir quality in carbonate rocks. Depositional facies is a significant factor in controlling the porosity and permeability of carbonate reservoirs, whereas diagenetic modifications not only change the primary compositions but also affect the porosities and permeabilities of the rock, due to neomorphism, cementation, micritization, compaction, dolomitization and dissolution. These diagenetic alterations may either enhance the reservoir quality, or occlude the porosity and permeability of carbonate rock (Moore and Wade, 2013). The petrographic studies revealed the depositional processes have produced

fenestral porosity in mudstone and wackestone of peritidal and lagoonal origin, while the rest of the microfacies have not recorded any primary porosity. The fenestrae are penecontemporaneous open spaces in the rock framework, which are larger in size than grain-supported pore spaces (Flügel, 2004). The fenestral fabric formed in peritidal settings as a result of (1) shrinkage and expansion, (2) air escape during flooding, (3) gas bubbling and (4) wrinkling of algal mats (Shinn, 1968). Such kinds of porosities were common during the Regressive Systems Tracts (RSTs), which have deposited mudstone to wackestone textural attributes in the studied unit. In Transgressive Systems Tracts (TSTs), the early heavy cementations in carbonate shoals have occluded the primary porosity in packstone and grainstone facies (Bathurst, 1987; Flügel, 2004).

The Samana Suk Formation in the Kohat Range is highly fractured, as a result of multiple phases of deformation (e.g. Gilmour et al., 1981), which have ultimately modified the reservoir behavior of the unit. Apart from fracturing, macroscopic dissolution in the form of molds and vugs have further enhanced the porosity in the unit. Moreover, the dissolution of bioclasts and dolomite has significantly increased porosity and permeability (Fig. 7k–l). It was observed that early and late-stage cementation played the most destructive role pertaining to porosity and permeability. In the early stages, the mechanical compaction has reduced intergranular porosity, with later cementation by blocky and granular cement further obliterating the reservoir properties. In the Samana Suk Formation, the chemical compaction phenomenon has caused the formation of low to high amplitude stylolites to suture seams and contacts. In general, chemical compaction

causes a reduction in porosity (Moore and Wade, 2001), but in the study area, it was observed that at places the dissolution of stylolites has enhanced porosity and permeability. Dolomitization in the Samana Suk Formation has significantly increased the intercrystalline porosity and permeability (Fig. 7m), but in some dolomites it was observed that the dolomite rhombs were tightly packed, which occluded the intercrystalline porosity (Fig. 7n). Moreover, late-stage calcite cementation in the dolomites has reduced the reservoir properties. Overall dissolution and dolomitization helped in enhancing the reservoir properties, whereas compaction and cementation have reduced the reservoir behavior.

The petrographic and plug porosity and permeability data indicate that the packstone and grainstone facies of carbonate shoals corresponding to TSTs have recorded higher porosities and permeabilities, as compared to the mudstone and wackestone of peritidal and lagoonal settings. The mudstone with pervasive dolomitization has recorded higher porosity, both in petrographic studies as well as in plug porosity. Although the primary fenestral porosities were recorded within the RSTs, diagenetic dissolution dominates the grainstone microfacies. These findings are in contrast to the higher dissolution porosities recorded within the mudstone and wackestone microfacies (deposited in RSTs) of the Samana Suk Formation in the Kala Chitta Range (e.g. Wadood et al., 2021a). The dissolution within the mudstone and wackestone facies of the Samana Suk Formation in the Kala Chitta Range has resulted mainly from methane exhalation as a result of decomposition of algae as well as dissolution of the same facies in association with grainstone occurring during burial diagenesis (Wadood et al., 2021a, b). The dominance of grainstone facies in the present study and mudstone to wackestone in Kala Chitta is the main reason for the contrasting porosities across the Samana Suk Formation. Based on the thickness and facies variations of the Samana Suk Formation, the shoreline is proposed to have been located in the northeast-southwest direction, with the ramp deepening towards the west (e.g. Saboor et al., 2020; Wadood et al., 2021a). Kala Chitta falls in the eastern relatively shallow part of the ramp and has therefore recorded peritidal and lagoonal facies, in contrast to the studied section. The intense selective dissolution in the allochems has intracortical, intraparticle and moldic porosity development within ooids and other allochems in grainstone microfacies during both meteoric and burial dissolution. The primary intergranular porosity in the ooidal shoals and skeletal wackestone and grainstone facies, shoal exposure and recharge of freshwater and subsequent dissolution as well as burial dissolution, enhances their reservoir potential (see e.g., Wenzhi et al., 2014; Beigi et al., 2017).

6 Conclusions

The Samana Suk Formation in the Kohat Range is comprised of thin to thick-bedded, oolitic, bioclastic, dolomitic and fractured limestone. Based on 16

microfacies, the Samana Suk Formation is deposited on a gently sloping homoclinal ramp, ranging from peritidal to carbonate shoals. The sequence stratigraphy investigation divulged a total of seven TSTs and six RSTs in the rock unit. The Samana Suk Formation was subjected to various diagenetic environments, with modifications of carbonates in the form of physical and mechanical compaction, cementation, micritization, dissolution and dolomitization. The integrated porosity and permeability analyses revealed that good, moderate and poor reservoir potential for high energy shoal (TST deposits), lagoonal (RST deposits) and peritidal facies (RST deposits) were respectively recorded. The diagenetic dolomitization and dissolution enhanced reservoir behavior, whereas cementation and compaction obliterated the reservoir properties.

Acknowledgments

The authors are thankful to the staff and faculty of the Department of Earth Sciences of Quaid-i-Azam University, Islamabad, particularly to Dr Aamir Ali, the Chairperson and Associate Professor at the department for his continuous support throughout the Ph.D. The authors are thankful to the National Center of Physics, Islamabad, for conducting the XRD analyses. Moreover, the authors thank Syed Waseem Sajjad, Ph.D. Scholar at Quaid-i-Azam University, Islamabad, for their assistance during fieldwork. The authors are also grateful to the anonymous reviewers for their technical and constructive suggestions for improving the manuscript.

Manuscript received Sep. 30, 2020

accepted Apr. 11, 2022

associate EIC: ZHANG Shuichang

edited by Jeffery J. LISTON and FANG Xiang

References

- Addi, A.A., and Chafiki, D., 2013. Sedimentary evolution and palaeogeography of mid-Jurassic deposits of the Central High Atlas, Morocco. *Journal of African Earth Sciences*, 84: 54–69.
- Afife, M.M., Sallam, E.S., and Faris, M., 2017. Integrated petrophysical and sedimentological study of the Middle Miocene Nullipore Formation (Ras Fanar Field, Gulf of Suez, Egypt): An approach to volumetric analysis of reservoirs. *Journal of African Earth Sciences*, 134: 526–548.
- Ahmad, F., Quasim, M.A., and Ahmad, A.H.M., 2020. Lithofacies characteristics and depositional environment interpretations of the Middle Jurassic Fort Member rocks, Jaisalmer Formation, Western Rajasthan, India. *Journal of Sedimentary Environments*, 5(3): 355–373.
- Al-Aasm, I.S., and Packard, J.J., 2000. Stabilization of early-formed dolomite: A tale of divergence from two Mississippian dolomites. *Sedimentary Geology*, 131(3): 97–108.
- Ali, A., Wagreich, M., and Strasser, M., 2018. Depositional constraints and diagenetic pathways controlling petrophysics of Middle Miocene shallow-water carbonate reservoirs (Leitha limestones), Central Paratethys, Austria-Hungary. *Marine and Petroleum Geology*, 91: 586–598.
- Amel, H., Jafarian, A., Husinec, A., Koeshidayatullah, A., and Swennen, R., 2015. Microfacies, depositional environment and diagenetic evolution controls on the reservoir quality of the Permian Upper Dalan Formation, Kish Gas Field, Zagros Basin. *Marine and Petroleum Geology*, 67: 57–71.
- Ayyıldız, T., Tekin, E., and Friedman, G.M., 2001. Microtextural properties of ooids in the Middle Jurassic-Lower Cretaceous, Central Taurus carbonate platform,

- Antalya, Turkey. Carbonates and Evaporites, 16(1): 1–7.
- Azerêdo, A.C., Inês, N., and Bizarro, P., 2020. Carbonate reservoir outcrop analogues with a glance at pore-scale (Middle Jurassic, Lusitanian Basin, Portugal). *Marine and Petroleum Geology*, 111: 815–851.
- Azmy, K., Knight, I., Lavoie, D., and Chi, G., 2009. Origin of dolomites in the Boat Harbour Formation, St. George Group, in western Newfoundland, Canada: Implications for porosity development. *Bulletin of Canadian Petroleum Geology*, 57(1): 81–104.
- Bachmann, M., and Hirsch, F., 2006. Lower Cretaceous carbonate platform of the eastern Levant (Galilee and the Golan Heights): Stratigraphy and second-order sea-level change. *Cretaceous Research*, 27(4): 487–512.
- Bathurst, R.G., 1987. Diagenetically enhanced bedding in argillaceous platform limestones: Stratified cementation and selective compaction. *Sedimentology*, 34(5): 749–778.
- Bathurst, R.G.C., 1983. Early diagenesis of carbonate sediments. In: Parker, A., and Sellwood, B.W. (eds.), *Sediment Diagenesis*. Springer, D. Reidel Publishing Company, 349–377.
- Beigi, M., Jafarian, A., Javanbakht, M., Wanas, H.A., Mattern, F., and Tabatabaei, A., 2017. Facies analysis, diagenesis and sequence stratigraphy of the carbonate-evaporite succession of the Upper Jurassic Surmeh Formation: Impacts on reservoir quality (Salman Oil Field, Persian Gulf, Iran). *Journal of African Earth Sciences*, 129: 179–194.
- Booler, J., and Tucker, M.E., 2002. Distribution and geometry of facies and early diagenesis: The key to accommodation space variation and sequence stratigraphy: Upper Cretaceous Congost Carbonate platform, Spanish Pyrenees. *Sedimentary Geology*, 146(3–4): 225–247.
- Bosence, D., Procter, E., Aurell, M., Bel Kahla, A., Boudagher-Fadel, M., Casaglia, F., Cirilli, S., Mehdie, M., Nieto, L., Rey, J., Scherreiks, R., Soussi, M., and Waltham, D., 2009. A dominant tectonic signal in high-frequency, peritidal carbonate cycles? A regional analysis of Liassic platforms from Western Tethys. *Journal of Sedimentary Research*, 79(6): 389–415.
- Bossart, P., Dietrich, D., Greco, A., Ottiger, R., and Ramsay, J.G., 1988. The tectonic structure of the Hazara-Kashmir Syntaxis, southern Himalayas, Pakistan. *Tectonics*, 7(2): 273–297.
- Brigaud, B., Durlot, C., Deconinck, J.F., Vincent, B., Pucéat, E., Thierry, J., and Trouiller, A., 2009. Facies and climate/environmental changes recorded on a carbonate ramp: A sedimentological and geochemical approach on Middle Jurassic carbonates (Paris Basin, France). *Sedimentary Geology*, 222(3–4): 181–206.
- Chatterjee, R., 2013. Physiological attributes of tomato (*Lycopersicon esculentum* Mill.) influenced by different sources of nutrients at foothill of eastern Himalayan region. *Journal of Applied and Natural Science*, 5(2): 282–287.
- Chatterjee, S., and Scotese, C., 2010. The wandering Indian plate and its changing biogeography during the Late Cretaceous–Early Tertiary period. In: *New aspects of Mesozoic biodiversity*, Lecture Notes in Earth Sciences, Volume 132. Berlin-Heidelberg: Springer, 105–126.
- Chen, D., Qing, H., and Yang, C., 2004. Multistage hydrothermal dolomites in the Middle Devonian (Givetian) carbonates from the Guilin area, South China. *Sedimentology*, 51(5): 1029–1051.
- Choquette, P.W., and Pray, L.C., 1970. Geologic nomenclature and classification of porosity in sedimentary carbonates. *AAPG bulletin*, 54(2): 207–250.
- Conliffe, J., Azmy, K., and Greene, M., 2012. Dolomitization of the Lower Ordovician Catoche Formation: Implications for hydrocarbon exploration in western Newfoundland. *Marine and Petroleum Geology*, 30(1): 161–173.
- Coward, M.P., and Butler, R.W.H., 1985. Thrust tectonics and the deep structure of the Pakistan Himalaya. *Geology*, 13(6): 417–420.
- Dickson, J.A.D., 1965. A modified staining technique for carbonates in thin section. *Nature*, 205(4971): 587–587.
- Ding, Y., Chen, D., Zhou, X., Guo, C., Huang, T., and Zhang, G., 2019. Tectono-depositional pattern and evolution of the middle Yangtze Platform (South China) during the late Ediacaran. *Precambrian Research*, 333: 105426.
- Drivet, E., and Mountjoy, E.W., 1997. Dolomitization of the Leduc Formation (Upper Devonian), southern Rimbey-Meadowbrook reef trend, Alberta. *Journal of Sedimentary Research*, 67(3): 411–423.
- Dunham, R.J., 1962. Classification of carbonate rocks according to depositional textures. In: Ham, W.E. (ed.), *Classification of carbonate rocks: A symposium (Vol. 1)*. American Association of Petroleum Geologists Memoir, Tulsa, 38: 108–121.
- El-Sorogy, A., Al-Kahtany, K., Almadani, S., and Tawfik, M., 2018. Depositional architecture and sequence stratigraphy of the Upper Jurassic Hanifa Formation, central Saudi Arabia. *Journal of African Earth Sciences*, 139: 367–378.
- Embry, A.F., and Johannessen, E.P., 2017. Two approaches to sequence stratigraphy. In: *Stratigraphy and Timescales*, 2: 85–118.
- Emery, D., and Myers, K., 1996. *Sequence stratigraphy*. Blackwell Scientific Publications, 1–297.
- Flügel, E., 2004. *Microfacies of carbonate rocks: Analysis, interpretation and application (1st ed.)*. Springer Science & Business Media.
- Flügel, E., 2010. *Microfacies of carbonate rocks: Analysis, interpretation and application (2nd ed.)*. Springer-Verlag.
- Friedman, G.M., 1965. Terminology of crystallization textures and fabrics in sedimentary rocks. *Journal of Sedimentary Research*, 35(3): 643–655.
- Gansser, A., 1981. The geodynamic history of the Himalaya. In: Gupta, H.K., and Delany, F.M. (eds.), *Zagros Hindu Kush Himalaya Geodynamic Evolution*, Geodynamics Series, Volume 3, American Geophysical Union, 1–323.
- Gilmour, E.H., Mughal, M.A., Sarhan, A.G., and Rahman, U.O., 1981. Carbonate petrography and microfacies of a portion of the Samana Suk Formation, Kohat Range, Pakistan. *Geological Bulletin, University of Peshawar*, 14: 73–84.
- Gischler, E., Birgel, D., Brunner, B., and Peckmann, J., 2020. Microbialite occurrence and patterns in Holocene reefs of Bora Bora, Society Islands. *Palaios*, 35(6): 262–276.
- Greco, A., Martinotti, G., Papritz, K., Ramsay, J.G., and Rey, R., 1989. The crystalline rocks of the Kaghan Valley (NE-Pakistan). *Eclogae Geologicae Helvetiae*, 82(2): 629–653.
- Guo, C., Chen, D., Qing, H., Dong, S., Li, G., Wang, D., Qian, Y., and Liu, C., 2016. Multiple dolomitization and later hydrothermal alteration on the Upper Cambrian–Lower Ordovician carbonates in the northern Tarim Basin, China. *Marine and Petroleum Geology*, 72: 295–316.
- Ham, W.E. (ed.), 1962. *Classification of carbonate rocks: A symposium*. American Association of Petroleum Geologists, Tulsa, Memoir 1, 1–279.
- Handford, C.R., and Loucks, R.G., 1993. Carbonate depositional sequences and systems tracts—responses of carbonate platforms to relative sea-level changes. In: Loucks, R.G., and Sarg, J.F. (eds.), *Carbonate sequence stratigraphy: Recent developments and applications*. American Association of Petroleum Geologists Memoir, 57: 3–41.
- Haq, B.U., Hardenbol, J., and Vail, P.R., 1988. Mesozoic and Cenozoic chronostratigraphy and cycles of sea-level change. In: Wilgus, C.K., Hastings, B.S., Posamentier, H., Van Wagoner, J., Ross, C.A., and Kendall, C.G.St.C. (eds.), *Sea-level changes: An integrated approach*. SEPM Special Publication, 42: 71–108.
- Harris, P.M., 1979. *Facies anatomy and diagenesis of a Bahamian ooid shoal (Vol. 7)*. Comparative Sedimentology Laboratory, Division of Marine Geology and Geophysics, University of Miami, Rosenstiel School of Marine and Atmospheric Science, 1–163.
- Hashmie, A., Rostamnejad, A., Nikbakht, F., Ghorbanie, M., Rezaie, P., and Gholamalian, H., 2016. Depositional environments and sequence stratigraphy of the Bahram Formation (Middle–Late Devonian) in north of Kerman, south-central Iran. *Geoscience Frontiers*, 7(5): 821–834.

- Heerwagen, E., and Martini, R., 2020. The Vizcaíno terrane: Another occurrence of Upper Triassic shallow-marine carbonates in Mexico. *Facies*, 66(1): 8.
- Henderson, A.L., Najman, Y., Parrish, R., Mark, D. F., and Foster, G. L. 2011. Constraints on the timing of India-Eurasia collision; a re-evaluation of evidence from the Indus Basin sedimentary rocks of the Indus-Tsangpo Suture Zone, Ladakh, India. *Earth Science Reviews*, 106(3-4): 265-292.
- Hillgärtner, H., and Strasser, A., 2003. Quantification of high-frequency sea-level fluctuations in shallow-water carbonates: An example from the Berriasian-Valanginian (French Jura). *Palaeogeography, Palaeoclimatology, Palaeoecology*, 200(1-4): 43-63.
- Hollis, C., Bastesen, E., Boyce, A., Corlett, H., Gawthorpe, R., Hirani, J., Rotevatn, A., and Whitaker, F., 2017. Fault-controlled dolomitization in a rift basin. *Geology*, 45(3): 219-222.
- Hughes, G., 2009. Micropaleontology and paleoenvironments of Saudi Arabian Upper Permian carbonates and reservoirs. In: Thomas, D., Demchuk, T.D., and Gary, A.C. (eds.), *Geologic problem solving with microfossils: A volume in honor of Garry D. Jones*. SEPM Special Publication, 93: 111-126.
- Hussain, H.S., Fayaz, M., Haneef, M., Hanif, M., Jan, I.U., and Gul, B., 2013. Microfacies and diagenetic-fabric of the Samana Suk Formation at Harnoi Section, Abbottabad, Khyber Pakhtunkhwa, Pakistan. *Journal of Himalayan Earth Science*, 46(2): 79-91.
- Hussein, D., Collier, R., Lawrence, J.A., Rashid, F., Glover, P.W.J., Lorinczi, P., and Baban, D.H., 2017. Stratigraphic correlation and paleoenvironmental analysis of the hydrocarbon-bearing Early Miocene Euphrates and Jeribe formations in the Zagros folded-thrust belt. *Arabian Journal of Geosciences*, 10(24): 1-15.
- Insalaco, E., Virgone, A., Courme, B., Gaillot, J., Kamali, M., Moallemi, A., Lotfpour, M., and Monibi, S., 2006. Upper Dalan Member and Kangan Formation between the Zagros Mountains and offshore Fars, Iran: Depositional system, biostratigraphy and stratigraphic architecture. *GeoArabia*, 11 (2): 75-176.
- Jadoon, I.A.K., 1992. Ocean/continental transitional crust underneath the Sulaiman Thrust Lobe and an evolutionary tectonic model for the Indian/Afghan Collision Zone. *Pakistan Journal of Hydrocarbon Research*, 4(2): 33-44.
- Jan, M.Q., and Asif, M., 1981. A speculative tectonic model for the evolution of NW Himalaya and Karakoram. *Geological Bulletin of the University of Peshawar*, 14: 199-201.
- Jank, M., Wetzel, A., and Meyer, C.A., 2006. Late Jurassic sea-level fluctuations in NW Switzerland (Late Oxfordian to Late Kimmeridgian): Closing the gap between the Boreal and Tethyan realm in Western Europe. *Facies*, 52(4): 487-519.
- Kadri, I.B., 1995. *Petroleum Geology of Pakistan*. Pakistan Petroleum Limited, 1-275.
- Kakemem, U., Jafarian, A., Husinec, A., Adabi, M.H., and Mahmoudi, A., 2021. Facies, sequence framework, and reservoir quality along a Triassic carbonate ramp: Kangan Formation, South Pars Field, Persian Gulf Superbasin. *Journal of Petroleum Science and Engineering*, 198: 108166
- Karimi, H., Ghadimvand, N., and Abdolhosein, K., 2015. Sedimentary environment and sequence stratigraphy of the Kangan Formation in Kish Gas Field (Kish Well A1 subsurface section). *Indian Journal of Science and Technology*, 8(7): 655-663.
- Kazmi, A.H., and Rana, R.A. 1982. Tectonic map of Pakistan 1: 2 000 000: Map showing structural features and tectonic stages in Pakistan. Geological survey of Pakistan.
- Ullah Khan, E., Saleem, M., Naseem, A.A., Ahmad, W., Yaseen, M., and Khan, T.U., 2020. Microfacies analysis, diagenetic overprints, geochemistry, and reservoir quality of the Jurassic Samanasuk Formation at the Kahi Section, Nizampur Basin, NW Himalayas, Pakistan. *Carbonates and Evaporites*, 35(95): 95.
- Khan, E.U., Naseem, A.A., Saleem, M., Rehman, F., Sajjad, S.W., Ahmad, W., and Azeem, T., 2021. Petrography and geochemistry of dolomites of Samanasuk Formation, Dara Adam Khel Section, Kohat Ranges, Pakistan. *Sains Malaysiana*, 50(11): 3205-3217.
- Khan, M.A., Ahmed, R., Raza, H.A., and Kemal, A., 1986. Geology of petroleum in Kohat-Potwar Depression, Pakistan. *AAPG Bulletin*, 70(4): 396-414.
- Khan, S.D., Walker, J., Hall, S., Burke, K.C., Shah, M., and Stockli, L., 2009. Did Kohistan-Ladakh island arc collide first with India? *Geological Society American Bulletin*. Geological Society of America Bulletin, 121(4): 366-384.
- Lasemi, Y., Jahani, D., Amin-Rasouli, H., and Lasemi, Z., 2012. Ancient carbonate tidalites. In: Davis, R.Jr., and Dalrymple, R. (eds.), *Principles of tidal sedimentology*, Dordrecht: Springer, 567-607.
- Lazăr, I., Grădinaru, M., and Petrescu, L., 2013. Ferruginous microstromatolites related to Middle Jurassic condensed sequences and hardgrounds (Bucegi Mountains, Southern Carpathians, Romania). *Facies*, 59(2): 359-390.
- Le Fort, P., 1975. Himalayas: The collided range. Present knowledge of the continental arc. *American Journal of Science*, 275(1): 1-44.
- Leech, M.L., Singh, S., Jain, A.K., Klemperer, S.L., and Manickavasagam, R.M., 2005. The onset of India-Asia continental collision: Early, steep subduction required by the timing of UHP metamorphism in the western Himalaya. *Earth and Planetary Science Letters*, 234(1): 83-97.
- Loreau, J.P., and Purser, B.H., 1973. Distribution and ultrastructure of Holocene ooids in the Persian Gulf. In: Purser, B.H. (ed.), *The Persian Gulf*. Springer, 279-328.
- Masood, H., 1989. Samana Suk Formation depositional and diagenetic history. *Kashmir Journal of Geology*, 6: 151-161.
- Mazzullo, S.J., 1992. Geochemical and neomorphic alteration of dolomite: A review. *Carbonates and Evaporites*, 7(1): 21-37.
- Meissner, J.C.R., Master, J.M., Rashid, M.A., and Hussain, M., 1974. Stratigraphy of the Kohat Quadrangle, Pakistan. In: Professional Paper (No. 716-D). U.S.: Government Printing Office.
- Molnar, P., and Qidong, D., 1984. Faulting associated with large earthquakes and the average rate of deformation in central and eastern Asia. *Journal of Geophysical Research: Solid Earth*, 89(7): 6203-6227.
- Molnar, P., and Tapponnier, P., 1975. Cenozoic tectonics of Asia: Effects of a continental collision. *Science*, 189(4201): 419-426.
- Montanez, I.P., and Read, J.F., 1992. Fluid-rock interaction history during stabilization of early dolomites, upper Knox Group (Lower Ordovician), U.S. Appalachians. *Journal of Sedimentary Research*, 62(5): 753-778.
- Montaron, B., 2008. Confronting carbonates. *Oil Review Middle East*, 5: 132-135.
- Moore, C.H., and Wade, W.J., 2001. Carbonate reservoirs: Porosity. Evolution and diagenesis in a sequence stratigraphic framework.
- Moore, C.H., and Wade, W.J., 2013. Carbonate reservoirs: Porosity and diagenesis in a sequence stratigraphic framework (2nd edition). Newnes, 392.
- Morad, S., 1998. Carbonate cementation in sandstones: Distribution patterns and geochemical evolution, 1-26.
- Morad, S., Ketzer, J.M., and De Ros, L.F., 2000. Spatial and temporal distribution of diagenetic alterations in siliciclastic rocks: Implications for mass transfer in sedimentary basins. *Sedimentology*, 47: 95-120.
- Morad, S., Ketzer, J., and DeRos, L., 2012. Linking diagenesis to sequence stratigraphy: An integrated tool for understanding and predicting reservoir quality distribution. In: Morad, S., Ketzer, J., and DeRos, L. (eds.), *Linking diagenesis to sequence stratigraphy*. Special Publication International Association Sedimentologists, 45: 1-36.
- Nazari, M.H., Tavakoli, V., Rahimpour-Bonab, H., and Sharifi-Yazdi, M., 2019. Investigation of factors influencing geological heterogeneity in tight gas carbonates, Permian reservoir of the Persian Gulf. *Journal of Petroleum Science and Engineering*, 183: 106341.
- Ni, J., and Barazangi, M., 1985. Active tectonics of the western Tethyan Himalaya above the underthrusting Indian Plate: the Upper Sutlej River Basin as a pull-apart structure. *Tectonophysics*, 112(1-4): 277-295.

- Nizami, A.R., 2008. Sedimentology of the Middle Jurassic Samanasuk Formation in Trans Indus Ranges Pakistan (Doctoral thesis). Lahore: University of Punjab.
- Powell, C.M., 1979. A speculative tectonic history of Pakistan and surroundings: Some constraints from the Indian Ocean. *Geodynamics of Pakistan*, 13: 5–24.
- Powell, C.M., and Conaghan, P.J., 1973. Plate tectonics and the Himalayas. *Earth and Planetary Science Letters*, 20(1): 1–12.
- Purser, B.H., and Evans, G., 1973. Regional sedimentation along the Trucial Coast, SE Persian Gulf. In: Purser, B.H. (ed.), *The Persian Gulf*. Springer, 211–231.
- Qureshi, M.K.A., Butt, A.A., and Ghazi, S., 2008. Shallow shelf sedimentation of the Jurassic Samana Suk Limestone, Kala Chitta Range, Lesser Himalayas, Pakistan. *Geological Bulletin Punjab University*, 43: 1–14.
- Rasser, M., Scheibner, C., and Mutti, M., 2005. A paleoenvironmental standard section for Early Herdian tropical carbonate factories (Corbieres, France; Pyrenees, Spain). *Facies*, 51: 218–232.
- Read, J.F., and Horbury, A.D., 1993. Diagenesis and porosity evolution associated with metre-scale disconformities and sequence bounding unconformities. *Diagenesis and basin development*, 36: 155–197.
- Rehman, H.U., Seno, T., Yamamoto, H., and Khan, T., 2011. Timing of collision of the Kohistan–Ladakh Arc with India and Asia: Debate. *Island Arc*, 20(3): 308–328.
- Reid, R.P., and Macintyre, I.G., 2000. Microboring versus recrystallization in shallow marine carbonates, Mississippian Alida beds, Williston Basin (Canada): Evidence from petrography and isotope geochemistry. *Journal of Sedimentary Research*, 70(1): 24–28.
- Reolid, M., Gaillard, C., and Lathuilière, B., 2007. Microfacies, microtaphonomic traits and foraminiferal assemblages from Upper Jurassic oolitic–coral limestones: Stratigraphic fluctuations in a shallowing-upward sequence (French Jura, middle Oxfordian). *Facies*, 53(4): 553–574.
- Rott, C.M., and Qing, H.R., 2013. Early dolomitization and recrystallization in shallow marine carbonates, Mississippian Alida beds, Williston Basin (Canada): Evidence from petrography and isotope geochemistry. *Journal of Sedimentary Research* 83: 928–941.
- Rousseau, M., Dromart, G., Garcia, J.P., Atrops, F., and Guillocheau, F., 2005. Jurassic evolution of the Arabian carbonate platform edge in the central Oman Mountains. *Journal of the Geological Society*, 162(2): 349–362.
- Sabor, A., Haneef, M., Hanif, M., and Swati, M.A.F., 2020. Sedimentological attributes of the Middle Jurassic peloids-dominated carbonates of eastern Tethys, lesser Himalayas, Pakistan. *Carbonates and Evaporites*, 35(4): 1–17.
- Sarg, J.F., 1988. Carbonate sequence stratigraphy. In: Wigus, C.K., (ed.), *Sea-level change: An integrated approach*. SEPM Special Publication, 42: 155–181.
- Sattler, U., Immenhauser, A.M., Hillgartner, H., and Esteban, M., 2005. Characterization, lateral variability and lateral extent of discontinuity surfaces on a carbonate platform (Barremian to Lower Aptian, Oman). *Sedimentology*, 52: 339–361.
- Schlager, W., 1992. Sedimentology and sequence stratigraphy of reefs and carbonate platforms. In: Continuing education course note series. American Association Petroleum Geologists, (34): 1–71.
- Scholle, P.A., and Ulmer-Scholle, D.S., 2003. A color guide to the petrography of carbonate rocks: Grains, textures, porosity, diagenesis. American Association of Petroleum Geologists. 1–473.
- Scoffin, T.P., 1987. An introduction to carbonate sediments and rocks. Glasgow: Blackie, 1–274.
- Seeber, L., Armbruster, J.G., and Quittmeyer, R.C., 1981. Seismicity and continental subduction in the Himalayan arc. In: Gupta, H.K., and Delany, F.M. (eds.), *Zagros Hindu Kush Himalaya Geodynamic Evolution*, Geodynamics Series, Volume 3. American Geophysical Union, 1–323.
- Sellwood, B.W., Scott, J., Mikkelsen, P., and Akroyd, P., 1985. Stratigraphy and sedimentology of the Great Oolite Group in the Humbly Grove oilfield, Hampshire. *Marine and Petroleum Geology*, 2(1): 44–55.
- Shah, S.M.I., 2009. Stratigraphy of Pakistan. Geological Survey of Pakistan, Memoirs, 22–265.
- Sheikh, R.A., Qureshi, M.K.A., Ghazi, S., and Masood, K.R., 2001. Jurassic carbonate shelf deposition Abbottabad District Northern Pakistan. *Geological Bulletin Punjab University*, 36: 49–62.
- Shinn, E.A., 1968. Selective dolomitization of recent sedimentary structures. *Journal of Sedimentary Research*, 38 (2): 612–616.
- Shinn, E.A., 1983a. Birdseyes, Fenestrae, Shrinkage Pores, and Loferites: A Reevaluation. *SEPM Journal of Sedimentary Research*, 53(2): 619–628.
- Shinn, E.A., 1983b. Tidal flat environment. In: Carbonate depositional environments. AAPG Memoir, 33: 172–210.
- Shukla, V., and Friedman, G.M., 1983. Dolomitization and diagenesis in a shallowing-upward sequence: The Lockport Formation (middle Silurian). *Journal of Sedimentary Research*, 53: 703–717.
- Sibley, D.F., and Gregg, J.M., 1987. Classification of dolomite rock textures. *Journal of Sedimentary Research*, 57: 967–975.
- Tahirkheli, R.A.K., 1979. The India-Eurasia Suture Zone in Northern Pakistan: Synthesis and interpretation of recent data at plate scale. *Geodynamics of Pakistan*. Geological Survey of Pakistan Quetta, 125–130.
- Tahirkheli, R.A.K., 1982. Geology of the Himalaya, Karakoram and Hindukush in Pakistan. *Geological Bulletin*, University of Peshawar, 15: 1–51.
- Tavakoli, V., and Jamalian, A., 2018. Microporosity evolution in Iranian reservoirs, Dalan and Dariyan formations, the central Persian Gulf. *Journal of Natural Gas Science and Engineering*, 52: 155–165.
- Taylor, T.R., Giles, M.R., Hathon, L.A., Diggs, T.N., Braunsdorf, N.R., Birbiglia, G.V., Kittridge, M.G., Macaulay, C.I., and Espejo, I.S., 2010. Sandstone diagenesis and reservoir quality prediction: Models, myths, and reality. *AAPG Bulletin*, 94(8): 1093–1132.
- Tucker, M.E., 1993. Carbonate diagenesis and sequence stratigraphy. *Sedimentology Review*. In: Spence, G.H., and Tucker, M.E. (eds.). A proposed integrated multi-signature model for peritidal cycles in carbonates. *Journal of Sedimentary Research*, 77(10): 797–808.
- Tucker, M.E., and Wright, V.P., 2009. Carbonate sedimentology. John Wiley and Sons, 1–496.
- Tucker, M.E., and Wright, V.P., 1990. Carbonate sedimentology. Oxford: Blackwell Publishing Ltd., 1–482.
- Van Buchem, F., Razin, P., Homewood, P., Oterdoom, W., and Philip, J., 2002. Stratigraphic organization of carbonate ramps and organic-rich intrashelf basins: Natih Formation (Middle Cretaceous) of Northern Oman. *AAPG Bulletin*, 86(1): 21–53.
- Wadood, B., Khan, S., Khan, A., Khan, M.W., Liu, Y., Li, H., Ahmad, S., and Khan, A., 2021a. Diachroneity in the closure of the eastern Tethys Seaway: Evidence from the cessation of marine sedimentation in northern Pakistan. *Australian Journal of Earth Sciences*, 1–11.
- Wadood, B., Khan, S., Liu, Y., Li, H., and Rahman, A., 2021b. Investigating the impact of diagenesis on reservoir quality of the Jurassic shallow shelfal carbonate deposits: Kala Chitta Range, North Pakistan. Special Issue: Biodiversity and floral patterns in the course of Cenozoic climate change. *Geological Journal*, 56(2): 1167–1186.
- Wadood, B., Khan, S., Li, H., Liu, Y., Ahmad, S., and Jiao, X., 2021. Sequence stratigraphic framework of the Jurassic Samana Suk carbonate formation, North Pakistan: Implications for reservoir potential. *Arabian Journal for Science and Engineering*, 46(1): 525–542.
- Wanas, H.A., 2008. Cenomanian rocks in the Sinai Peninsula, northeast Egypt: Facies analysis and sequence stratigraphy. *Journal of African Earth Sciences*, 52: 125–38.
- Watney, W.L., Doveton, J.H., and Guy, W.J., 1998. Development and demonstration of an enhanced spreadsheet-based well log analysis software. Final report (No. DOE/PC/91008-12). Kansas Geological Survey, Lawrence, KS, United States.
- Wenzhi, Z., Anjiang, S., Jingao, Z., Xiaofang, W., and Junming, L., 2014. Types, characteristics, origin and exploration

- significance of reef-shoal reservoirs: A case study of Tarim Basin, NW China and Sichuan Basin, SW China. *Petroleum Exploration and Development*, 41(3): 283–293.
- Wetzel, A., Weissert, H., Schaub, M., and Voegelin, A.R., 2013. Sea-water circulation on an oolite-dominated carbonate system in an epeiric sea (Middle Jurassic, Switzerland). *Sedimentology*, 60(1): 19–35.
- Wilson, J.L., 1975. Carbonate facies in geologic history. Springer-Verlag, 1–471.
- Windley, B.F., 1983. Metamorphism and tectonics of the Himalaya. *Journal of the Geological Society*, 140(6): 849–865.
- Worden, R.H., Armitage, P.J., Butcher, A.R., Churchill, J.M., Csoma, A.E., Hollis, C., Lander, R.H., and Omma, J.E., 2018. Petroleum reservoir quality prediction: Overview and contrasting approaches from sandstone and carbonate communities. Geological Society of London, Special Publications, 435(1): 1–31
- Yeats, R.S., and Hussain, A., 1987. Timing of structural events in the Himalayan foothills of northwestern Pakistan. *Geological Society of America Bulletin*, 99(2): 161–176.
- Yeats, R.S., and Lawrence, R.D., 1982. Tectonics of the Himalayan thrust belt in northern Pakistan. In: U.S.–Pakistan workshop on marine sciences in Pakistan, Karachi, Pakistan, November, 11–16: 1–39.
- Yousif, I.M., Abdullatif, O.M., Makkawi, M.H., Bashri, M.A., and Abdulghani, W.M., 2018. Lithofacies, paleoenvironment and high-resolution stratigraphy of the D5 and D6 members of the Middle Jurassic carbonates Dhurma Formation, outcrop analog, central Saudi Arabia. *Journal of African Earth Sciences*, 139: 463–479.

About the first author



Emadullah KHAN, Male; received B.Sc. in Earth Sciences from COMSATS University, Abbottabad, then M.Sc. from the Department of Earth Sciences of Quaid i Azam University, Islamabad. He is a lecturer and head of the Department of Geology at Abdul Wali Khan University, Mardan. He is interested in the study of carbonate sedimentology, particularly paleoenvironments, paleoclimate, diagenesis and geochemical analysis.

Moreover, his research interests also include petroleum geology, biostratigraphy, remote sensing, data science and machine learning. E-mail: emadgeo@awkum.edu.pk.

About the corresponding author



Abbas Ali NASEEM, Male; received M.Sc. from the Department of Earth Sciences of Quaid i Azam University, Islamabad and Ph.D. from Kyungpook National University, South Korea. He is currently an associate professor at the Department of Earth Sciences, Quaid Azam University, Islamabad. Previously, he worked as an assistant professor at the Department of Geology of Bacha Khan University, Charsadda. He is interested in the study of

sedimentology, engineering geology, geochemistry, remote sensing, and geoheritage. E-mail: abbasaliqau@gmail.com.